CO-SPUTTERED COPPER-DOPED ZINC OXIDE THIN FILMS

BY

SAEED ABDULLAH SAEED BAQRAF

A Thesis Presented to the
DEANSHIP OF GRADUATE STUDIES

KING FAHD UNIVERSITY OF PETROLEUM & MINERALS
DHAHRAN, SAUDI ARABIA

In Partial Fulfillment of the
Requirements for the Degree of

MASTER OF SCIENCE

In

PHYSICS

MAY 2017

KING FAHD UNIVERSITY OF PETROLEUM & MINERALS

DHAHRAN- 31261, SAUDI ARABIA

DEANSHIP OF GRADUATE STUDIES

This thesis, written by **SAEED ABDULLAH SAEED BAQRAF** under the direction his thesis advisor and approved by his thesis committee, has been presented and accepted by the Dean of Graduate Studies, in partial fulfillment of the requirements for the degree of **MASTER OF SCIENCE IN PHYSICS.**

Prof. Mohammad F. Al-Kuhaili
(Advisor)

Dr. Abdullah A. Al-Sunaidi
Department Chairman

Prof. Sardar M. Durrani
(Member)

Dr. Salam A. Zummo
Dean of Graduate Studies

Prof. Akhtar A. Naqvi
(Member)

1/6/17
Date

To my late father, my mother,

my brothers and my sisters

ACKNOWLEDGMENTS

In the name of Allah, the most Gracious and the most Merciful. Alhamdulillah, who supplied me with the courage, blessings and the guidance to complete this work successfully. Peace and blessings of Almighty Allah be upon the prophet Muhammad peace be upon him.

I submit my highest appreciation and thanks to my thesis advisor Prof. Mohammad F. Al-Kuhaili. My heartfelt thanks go to him for his high morals, support, high cooperation, inspiring encouragement and excellent technical guidance through the thesis. I am deeply indebted to him and without his help, knowledge skills and guidance, this work would not have been possible.

Deepest thanks and appreciation are also due to my committee members Prof. Sardar Mohammad Ayub Durrani and Prof. Akhtar A. Naqvi for their time and effort to read and examine my thesis. Special thanks go to them for their continuous encouragement and useful comments, I was lucky to have the chance of having them on my thesis committee.

I would like to acknowledge King Fahd University of Petroleum and Minerals for giving me the opportunity to complete my graduate studies in the Physics Department. My acknowledgment also goes to the Chairman Dr. Abdullah A. Al-Sunaidi, technicians and all staff members of the Physics Department for their help and co-operation.

I would like to appreciate the support offered by all my colleagues in the Physics Department. My most sincere thanks go to my best friends for their kindness and moral support during my study for the graduate program.

Last but not least, I would like to take this opportunity to give my deepest gratitude to my parents Abu Saeed (mercy on him) and Um Saeed, brothers and sisters for their endless love, support, patience, prayers, help and encouragement throughout my M.S. program.

TABLE OF CONTENTS

ACKNOWLEDGMENTS ..... **V**

TABLE OF CONTENTS ..... **VII**

LIST OF TABLES ..... **X**

LIST OF FIGURES ..... **XI**

LIST OF ABBREVIATIONS ..... **XV**

ABSTRACT ..... **XVII**

ملخص الرسالة ..... **XIX**

CHAPTER 1 INTRODUCTION **1**

1.1 ZINC OXIDE **1**

1.1.1 CRYSTAL STRUCTURE OF ZINC OXIDE **1**

1.1.2 PROPERTIES OF ZINC OXIDE **4**

1.1.3 APPLICATIONS OF ZINC OXIDE **4**

1.2 COPPER **5**

1.3 COPPER-DOPED ZINC OXIDE **8**

1.4 BAND GAP **8**

1.5 LITERATURE REVIEW **9**

1.5.1 MAGNETRON CO-SPUTTERING **9**

1.5.2 SOL-GEL DIP-COATING PROCESS **10**

1.5.3 SPRAY PYROLYSIS TECHNIQUE **11**

1.5.4 OTHER TECHNIQUES 11

1.6 SCOPE OF WORK 13

CHAPTER 2 EXPERIMENTAL TECHNIQUE 14

2.1 SPUTTERING TECHNIQUE 14

2.1.1 DIRECT CURRENT MAGNETRON SPUTTERING 17

2.1.2 RADIO FREQUENCY MAGNETRON SPUTTERING 17

2.1.3 MAGNETRON CONFOCAL SPUTTERING 18

2.1.4 ADVANTAGES OF MAGNETRON SPUTTERING 18

2.2 THIN FILM DEPOSITION AND PROCESSING 21

2.3 CHARACTERIZATION TECHNIQUES 22

2.3.1 SURFACE MORPHOLOGICAL ANALYSIS 22

2.3.2 STRUCTURE ANALYSIS 25

2.3.3 CHEMICAL ANALYSIS 27

2.3.4 CHEMICAL COMPOSITION 30

2.3.5 OPTICAL MEASUREMENTS 32

CHAPTER 3 STRUCTURAL AND CHEMICAL CHARACTERISTICS 34

3.1 STRUCTURAL PROPERTIES 34

3.2 MORPHOLOGICAL PROPERTIES 39

3.3 CHEMICAL ANALYSIS 42

CHAPTER 4 OPTICAL CHARACTERISTICS 53

CHAPTER 5 ANNEALING IN OXYGEN 64

5.1 STRUCTURAL PROPERTIES 64

5.2 MORPHOLOGICAL PROPERTIES 65

5.3 OPTICAL PROPERTIES 65

5.4 ELECTRICAL PROPERTIES 66

5.5 CHEMICAL ANALYSIS 67

CHAPTER 6 CONCLUSIONS AND FUTURE SUGGESTIONS 78

6.1 CONCLUSIONS 78

6.2 SUGGESTIONS 80

REFERENCES 81

VITAE 89

LIST OF TABLES

Table 3.1. Physical properties of the films as functions of the DC power applied to the Cu target 36

Table 3.2. Copper concentration (x) as a function of DC power 45

Table 4.1. Band gap (E_g) tunability of ZnO thin films using elemental dopants 56

Table 4.2. Band gap (E_g) of the films as function of the DC power applied to the Cu target 58

Table 5.1. Physical properties of as-deposited and annealed thin films. 68

LIST OF FIGURES

Figure 1.1. Hexagonal wurtzite lattice of zinc oxide 3

Figure 1.2. Face centered cubic of elemental copper..... 7

Figure 2.1. Schematic diagram of a sputtering system 16

Figure 2.2. Schematic diagram of confocal sputtering system 20

Figure 2.3. A schematic diagram of an atomic force microscope..... 24

Figure 2.4. Schematic diagram of Bragg's law..... 26

Figure 2.5. Schematic diagram of the basic principle of XPS 29

Figure 2.6. Schematic diagram of the basic principle of X-Ray fluorescence..... 31

Figure 2.7. Schematic diagram of optical measurements of thin film 33

Figure 3.1. XRD patterns of the films. (a) Pure ZnO; (b)Copper-doped ZnO film deposited using co-sputtering with a 10-W DC power applied to the copper target. 37

Figure 3.2. XRD patterns of copper-doped ZnO films deposited using co-sputtering with DC powers of 12 – 18 W applied to the copper target. 38

Figure 3.3. Three-dimensional AFM micrographs of Cu-doped ZnO films deposited using co-sputtering. The DC power applied to the Cu target is indicated on each image. 40

Figure 3.4. Two-dimensional AFM micrographs of Cu-doped ZnO films deposited using co-sputtering. The DC power applied to the Cu target is indicated on each image. 41

Figure 3.5. A typical XPS survey scan of a copper-doped ZnO film deposited using co-sputtering with an 18-W DC power, showing the main constituents of the film. 46

Figure 3.6. XPS spectra of a co-sputtered film using 18-W DC power applied to the copper target, showing the Zn 2p core-level spectrum. 47

Figure 3.7. O1s XPS spectrum of a co-sputtered film using 18-W DC power applied to the copper target. The spectrum was resolved into its three components. The experimental spectrum is denoted by the open circles. 48

Figure 3.8. XPS spectra of a co-sputtered film using 18-W DC power applied to the copper target, showing the Cu 2p core-level spectrum. 49

Figure 3.9. XPS depth profile of a co-sputtered film using 18-W DC power applied to the copper target, showing the relative intensity of Zn as a function of etching time. 50

Figure 3.10. XPS depth profile of a co-sputtered film using 18-W DC power applied to the copper target, showing the relative intensity of Cu as a function of etching time. 51

Figure 3.11. XPS depth profile of a co-sputtered film using 18-W DC power applied to the copper target, showing the relative intensity of O as a function of etching time. 52

Figure 4.1. Measured normal incidence transmittance spectra of the films. 59

Figure 4.2. Measured normal incidence absorption spectra of the films. 60

Figure 4.3. Dependence of the absorption coefficient of the films on photon energy. 61

Figure 4.4. Tauc plots showing the dependence of the band gap of the films on photon energy. 62

Figure 4.5. Dependence of the band gap of the films on the atomic concentration of copper 63

Figure 5.1. Three-dimensional AFM micrographs of as-deposited and annealed thin films. The DC power applied to the Cu target was 18 W 69

Figure 5.2. Two-dimensional AFM micrographs of as-deposited and annealed thin films. The DC power applied to the Cu target was 18 W 70

Figure 5.3. Measured normal incidence transmittance spectra of the films deposited under an 18 W DC power and annealed in oxygen 71

Figure 5.4. Measured normal incidence absorption spectra of the films deposited under an 18 W DC power and annealed in oxygen. 72

Figure 5.5. Dependence of the absorption coefficient of the films deposited under an 18 W DC power and annealed in oxygen on photon energy. 73

Figure 5.6. Tauc plots showing the dependence of the band gap of the films deposited under an 18 W DC power and annealed in oxygen on photon energy 74

Figure 5.7. Details of the electric measurement system. (a) Geometry of the gold contacts. (b) Measurement circuit. 75

Figure 5.8. Current-Voltage curves of as-deposited sample (a) and annealed sample (b). 76

Figure 5.9. O1s XPS spectrum of an annealed thin film. The spectrum was resolved into its three components. The experimental spectrum is denoted by the open circles 77

LIST OF ABBREVIATIONS

UV	:	Ultraviolet
PLD	:	Pulsed Laser Deposition
VLS	:	Vapor-Liquid-Solid
CVD	:	Chemical Vapor Deposition
FCC	:	Forced-Centered Cubic
E_g	:	Energy Band Gap
E_v	:	Energy Valence Band
E_c	:	Energy Conduction Band
RF	:	Radio Frequency
DC	:	Direct Current
α	:	Absorption Coefficient
SPM	:	Scanning Probe Microscopy
PVD	:	Physical Vapor Deposition
sccm	:	Standard Cubic Centimeter Per Minute
rpm	:	Revolution Per Minute
XRD	:	X-Ray Diffraction
AFM	:	Atomic Force Microscopy

XRF	:	X-Ray Fluorescence
XPS	:	X-Ray Photoelectron Spectroscopy
E_b	:	Binding Energy
Φ	:	Work Function
E_k	:	Kinetic Energy
A	:	Absorbed Radiation
R	:	Reflected Radiation
S	:	Scattered Radiation
T	:	Transmitted Radiation
R_{rms}	:	Root-Mean-Square Surface Roughness
cps	:	Counts Per Second
SP	:	Spray Pyrolysis
RFS	:	Radio-Frequency Sputtering
MBE	:	Molecular Beam Epitaxy

ABSTRACT

Full Name : [SAEED ABDULLAH SAEED BAQRAF]

Thesis Title : [CO-SPUTTERED COPPER-DOPED ZINC OXIDE THIN FILMS]

Major Field : [PHYSICS]

Date of Degree : [May, 2017]

Zinc oxide is a wide band gap semiconductor that has found potential applications in ultraviolet optoelectronics. Its utilization in the visible range necessitates that its energy gap be reduced and tunable. In this work, this was achieved by doping ZnO thin films with copper by means of a co-sputtering technique, where the ZnO was radio-frequency sputtered and the copper was DC-sputtered. The copper concentration was controlled through the DC power applied to the copper target, where concentration up to 51 at% were attained, indicating heavy doping. The structural properties were investigated by X-ray diffraction and revealed the growth was oriented along the (002) direction of hexagonal ZnO for pure zinc oxide and films deposited under 10 W DC power. The films were deposited under higher DC powers were amorphous. The surface morphological properties of the films were investigated by atomic force microscopy. The films had columnar structure with a surface roughness that decreased with an increase in copper doping concentration. The chemical properties of the films were investigated by X-ray photoelectron spectroscopy and revealed that the elements were homogenously distributed through the thickness of the films. The optical properties of the films, including the absorption coefficient and the band gap, were investigated by spectrophotometric measurements. The resulting films exhibited large absorption in the visible with a considerable red shift in the band gap approaching a value of 0.57 eV compared to pure

ZnO. The deposited films under a DC power of 18 W were annealed in an oxygen atmosphere at the temperature of 400 ˚C. The annealing effects on the films were investigated by XRD, which revealed the amorphous structure of the films, and atomic force microscopy which showed that the surface roughness of the films was increased. The optical and electrical properties of the annealed films revealed that the band gap and resistivity of the films were decreased.

ملخص الرسالة

الاسم الكامل: سعيد عبدالله سعيد بقرف

عنوان الرسالة: صناعة طبقات رقيقة من أكسيد الزنك المخلوط بالنحاس بطريقة الترسيب الأيوني

التخصص: فيزيـــــاء

تاريخ الدرجة العلمية: مايو، ٢٠١٧

أكسيد الزنك هو من أشباه الموصلات ذات الفجوة واسعة النطاق التي وجدت لها عدة تطبيقات في الإلكترونيات الضوئية فوق البنفسجية. واستخدام هذا الأكسيد في النطاق المرئي يستلزم خفض طاقته والتحكم فيها. في هذا العمل، تحقق هذا العمل من خلال تنشيط الاغشية الرقيقة لأكسيد الزنك بالنحاس عن طريق تقنية الترسيب الأيوني، حيث وضع أكسيد الزنك على المصدر الكهربائي المتردد بينما وضع النحاس على المصدر الكهربائي المستمر. الخصائص التركيبة للطبقات كشفت ان الأفلام متبلورة في الطاقات الكهربائية المنخفضة بينما في الطاقات الكهربائية العالية تكون غير متبلورة. تمت دراسة خصائص السطوح بواسطة مجهر القوة الذرية، حيث وجد أن درجة الخشونة انخفضت مع ارتفاع تركيز النحاس في الأفلام. الخصائص الكيميائية للأفلام تمت دراستها بواسطة التحليل الطيفي الضوئي بالأشعة السينية، ووجد أن العناصر موزعة بشكل متجانس داخل الأفلام. من الناحية الضوئية تمت دراسة معامل الامتصاص وطاقة الفجوة، ووجد أن هذه الطبقات لها قدرة امتصاص عالية في المنطقة المرئية وانخفاض لطاقة الفجوة يقترب من ٠,٥٧ الكترون فولت. تم تسخين الأفلام ذات القدرة العالية ١٨ واط في بيئه محاطة بالأكسجين عند درجة حرارة ٤٠٠ درجة مئوية، حيث وجد أن طبقات هذه الأفلام غير متبلورة، وكشف مجهر القوة الذرية زيادة خشونة سطوح هذه الأفلام وأيضا أظهرت الخصائص الضوئية والكهربائية لهذه الأفلام انخفاض في طاقة الفجوة وكذلك في مقاومة هذه الأفلام.

CHAPTER 1

INTRODUCTION

Metal oxides are significantly important for many scientific fields such as materials science, chemistry, and physics. Technologically, oxides are utilized in the making of piezoelectric devices, fuel cells, sensors, microelectronic circuits, coatings against corrosion, and as catalysts [1]. Copper-Doped Zinc Oxide belongs to the metal oxides and has found significant applications in various scientific and technological fields.

1.1 ZINC OXIDE

The compound zinc oxide (ZnO) is a transparent n-type semiconductor having a wide band gap of 3.4 eV [2 - 4]. It is a combination of the group-IIB element Zn and the group-VI element O. It has a large exciton binding energy of 60 meV at room temperature. Naturally, zinc oxide occurs as the mineral zincite, but most zinc oxide is produced synthetically. Zinc oxide has a density of 5.61 g/cm^{3}, a molar mass of 81.38 g/mol and a boiling point of 2,360 $^{\circ}$C [2]. Zinc oxide is widely used as an additive in numerous materials and products. It has several favorable properties that make it an ideal candidate for a variety of applications and technical devices [3].

1.1.1 CRYSTAL STRUCTURE OF ZINC OXIDE

Zinc oxide naturally crystallizes in a hexagonal wurtzite- structure that belongs to the space group P63mc [3]. Each zinc ion (Zn^{2+}) is tetrahedrally bonded to four oxygen ions (O^{2-}), and

each oxygen ion (O^{2-}) is tetrahedrally bonded to four zinc ions (Zn^{2+}); as shown in figure 1.1 [2]. The tetrahedral coordination in ZnO results in piezoelectricity in and also plays a key role in its crystal growth. The lattice parameters of the hexagonal unit cell are a = 0.3296 nm and c = 0.52065 nm [2].

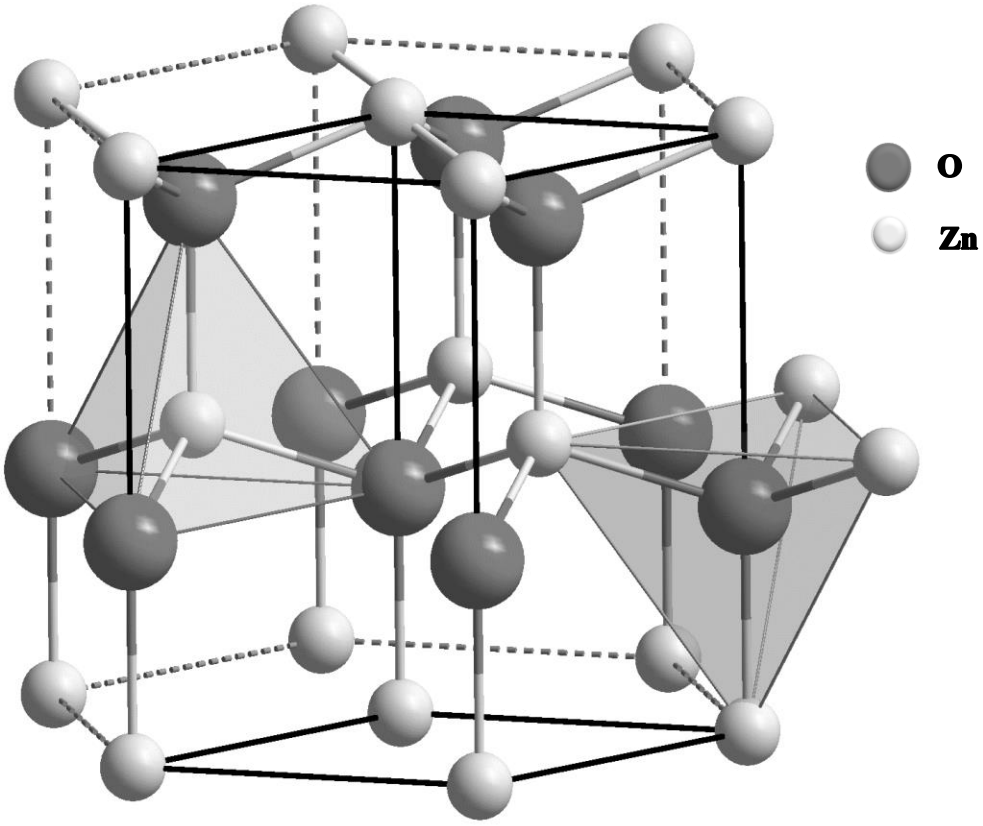

Figure 1.1. Hexagonal wurtzite lattice of zinc oxide

1.1.2 PROPERTIES OF ZINC OXIDE

Zinc oxide has excellent properties that give it great attention in theoretical and experimental sciences. It has high mechanical and chemical stability, it is nontoxic, and is cheaply available with a good abundance in nature [4 - 6]. ZnO is recognized as a promising photonic material in the blue–UV region. ZnO is a relatively soft material, with a hardness of ~5 GPa [3]. It has good electron mobility, excellent transparency and excellent room-temperature luminescence [7]. ZnO has a large band gap at room temperature and the characteristics associated with a wide band gap include higher breakdown voltages, ability to tolerate large electric fields and lower electronic noise. It has high a melting point of 1,975 ˚C, high heat capacity, high heat conductivity and low thermal expansion. Among semiconductors, ZnO exhibits the highest piezoelectric tensor and this property makes it a technologically important material for many piezoelectric applications [3, 7].

1.1.3 APPLICATIONS OF ZINC OXIDE

Recently, zinc oxide has an enormous application base, it has wide opportunities for industry and society alike due to its unique characteristics which are now being explored and applied. ZnO is investigated in solar cells, transparent transistor devices, ultraviolet laser diodes, blue luminescent devices, bipolar junction transistors, photodetectors, gas sensors and ultraviolet nanolasers [8 - 10]. Zinc oxide-based nanostructures, including nanowire arrays, are utilized for flat screen displays, field emission sources and chemical and biological sensors [3]. Epitaxial layers and single crystals will be important for the improvement of optoelectronic, piezoelectric and spintronic devices. Epitaxial ZnO also holds much promise as a semiconducting transparent thin film. Additionally, the radiation strength of zinc oxide to MeV proton irradiation makes it an ideal nominee for space applications [3]. Zinc oxide thin films have several physical

properties may be changed by different ways. These properties can be changed via several deposition techniques like pulsed laser deposition (PLD), molecular beam epitaxy, spray pyrolysis, vapor–liquid–solid (VLS), sol-gel method, chemical vapor deposition (CVD), and reactive magnetron sputtering. Also, zinc oxide properties can be altered by controlling the deposition parameters and annealing parameters like flow rate of gasses in the chamber, discharge the chamber, power sources, and temperature. Doping zinc oxide with different elements like Ga, Mg, Al, Br, Ti, In, and Cu could change the properties of ZnO, the doping method is the efficient method to change the properties of ZnO. In this work, our aim is to achieve substantial reduction and tunability of the band gap of radio-frequency-sputtered ZnO thin films through heavy doping with copper using the method of co-sputtering.

1.2 COPPER

Copper is one of the oldest metals used by man and belongs to the group of noble metals in the periodic table which also includes silver and gold. Copper is one of a few metals found in the native (metallic) form in nature. Copper is oxidized by air, especially in the presence of moisture at high temperatures. Copper is also oxidized in oxygenated water [11]. Copper interacts readily with many different bio-molecules and is an essential trace element in all living organisms [11]. Copper is an integrated part of our environment, both in pure form and as a mineral ore. The atomic structure of copper is $1s^{2}2s^{2}2p^{6}3s^{2}3p^{6}3d^{10}4s^{1}$ which indicates a filled 3d state and loosely bound 4s electrons. The optical transitions between the filled 3d and empty 4s states are responsible for the high electrical conductivity and thermal conductivity of copper and its distinctive red color. Copper exists in a single face-centered cubic (FCC) crystal form at all temperatures below its melting point as shown in figure 1.2 [12]**.** Copper offers low

electric resistivity, a high coefficient of thermal expansion, low thermal stability, low cost, high melting temperature, low rates of diffusivity and non-toxicity. Furthermore, copper has a wide range of mechanical properties, ease of deposition, fabricating, and joining [13, 14]. The significant properties of copper are high electrical conductivities and thermal conductivities. The other properties which make copper desirable in different applications are resistance to corrosion, aesthetic appeal, ease of machinability, strength combinations and ductility [15]. Primarily, copper oxide exists in two structures. The first oxidation state is a copper (I) oxide (Cu_2O). Cuprous oxide (Cu_2O) occurs in red color and has a bulk band gap of approximately 2.1 eV. The second oxidation state is copper (II) oxide (CuO). Cupric oxide (CuO) occurs in black color with a bulk band gap of approximately 1.85 eV. Copper oxides can be used for a number of applications which are gas sensors, lithium ion batteries, photovoltaic devices, photodetectors, photocatalysis, supercapacitors, and enzyme-free glucose sensors. [14, 16].

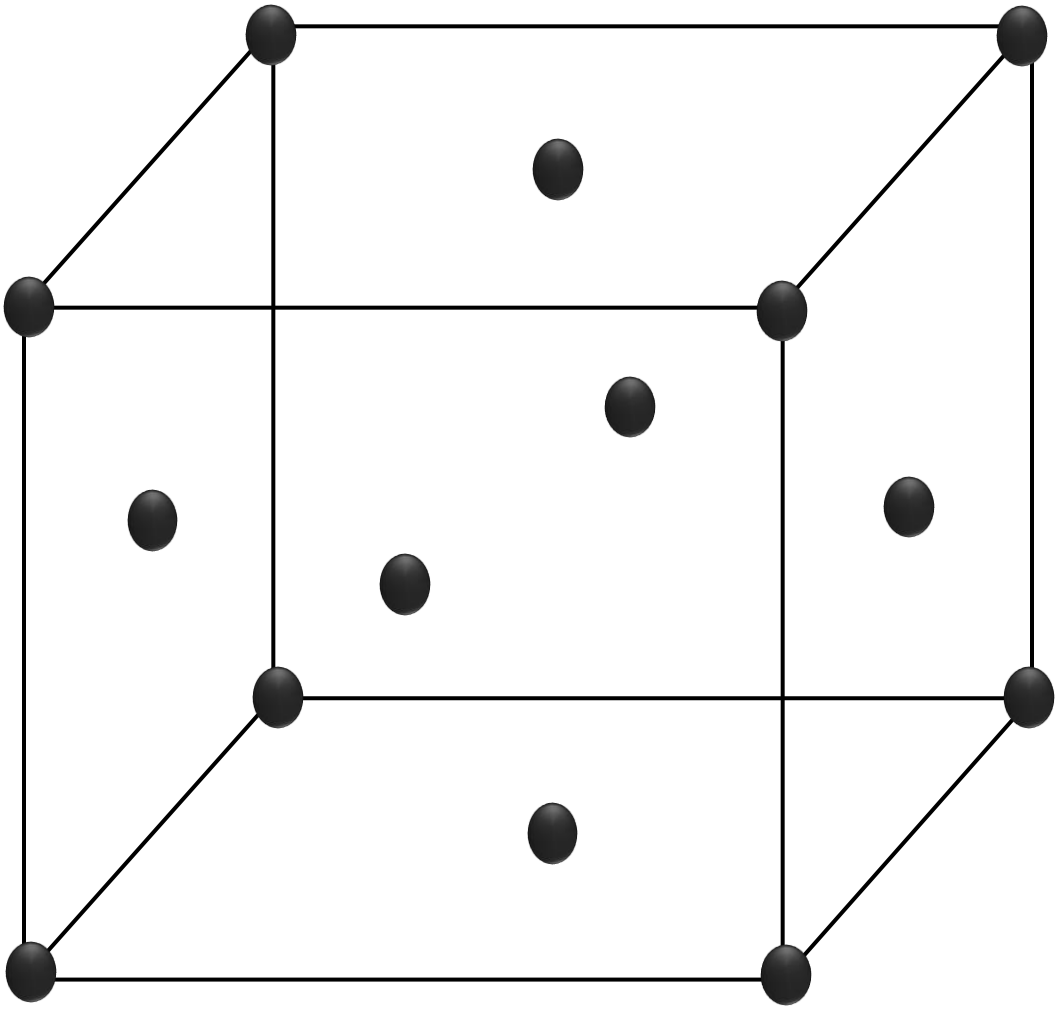

Figure 1.2. Face centered cubic of elemental copper

1.3 COPPER-DOPED ZINC OXIDE

Copper has been recognized as an ideal dopant in ZnO for various potential applications [17, 18]. There are several reasons for this. First, copper and zinc atoms have similar in different chemical and physical properties, non-toxicity, similar ionic radius and electronic shell structure [6, 17 - 19] , thus Cu can be easily incorporated in to the zinc oxide lattice, the incorporation of copper has strong influences on the structure, chemical, optical, and magnetic characteristics of ZnO [20 - 22]. Second, copper behaves as an acceptor in ZnO with an energy level located at 0.17 eV below the bottom of the conduction band [23], making it a good candidate for p-type doping of zinc oxide [19]. Third, copper acts as a visible-light photoconduction activator in ZnO [24] by creating localized impurity levels in the band gap of zinc oxide [21]. Finally, since copper doped zinc oxide has a transition temperature above room temperature and is intrinsically non-magnetic, it is a promising material for spitronic applications [25] .The copper dopant can improve the absorption coefficient and reduce the band gap [8, 9].

1.4 BAND GAP

The main base of many solid devices including diode lasers, solar cells, and computer chips is semiconducting materials. A semiconductor is a material that has a low electrical conductivity at room temperature. However, the low electrical conductivity of a semiconductor can be enhanced by the input of energy. The energy band gap (E_g) of semiconductors can be defined as the energy difference between the top of the valence band (E_v) which is the highest energy band that is filled with electrons and the bottom of the conduction band (E_c) which is the next higher band that is empty from electrons. The band gap of a semiconductor is given by:

$$E_g = E_c - E_v \quad (1.1)$$

The reduction of the bandgap in zinc oxide is desirable because of the bandgap ZnO is too large for absorption of visible light so it is critical to reducing the band gap to achieve a higher absorption coefficient in the visible. The band gap of zinc oxide can be changed by either increasing or decreasing the size of crystallites. The band gap can be changed too by doping some of the impurities such as copper. There are two types of doping. The first one is when the impurities replace a host cation in its position in the crystal lattice site. The second type is when the impurities are placed in the interstices of the crystal structure [26]. The reduction in the band gap of zinc oxide by Cu impurities is attributed to the increasing of the copper concentration in the films. The reduction of the band gap in ZnO is due to the large hybridization of the Cu (3d) bands with the O (2p) bands.

1.5 LITERATURE REVIEW

A lot of research efforts have been devoted to copper-doped zinc oxide thin films due to plenty of applications. I will display the main synthesis techniques that have been utilized in the deposition of copper doped zinc oxide thin films.

1.5.1 MAGNETRON CO-SPUTTERING

Liu et al [19] used magnetron co-sputtering with high purity zinc oxide and copper targets to create heavily-doped (ZnO: Cu) thin films. They investigated the optical characteristics and microstructure properties of the thin films. They found that heavy copper doping decreased the grain size of the thin films, while moderate copper doping could promote the grain size of the films.

Kostruba et al [27] deposited copper-doped ZnO films by RF magnetron sputtering with a thickness about 1200 nm on glass substrates. They studied the surface morphology and the structure of the films and found that the crystalline structure of the thin films was not affected by a few percent of copper.

Sudakar et al [28] deposited copper-doped zinc oxide thin films by reactive magnetron co-sputtering with high metallic purity zinc and copper targets using (DC) power sources and (RF) power sources. The construction quality and magnetic characteristics of thin films grown on quartz and sapphire substrates showed that the combination of copper into zinc oxide lattice did not change the crystal structure.

1.5.2 SOL-GEL DIP-COATING PROCESS

Saidani et al [29] prepared un-doped and copper-doped zinc oxide films on glass substrates by sol–gel dip-coating process. They studied the structural and optical characteristics of the (Cu: ZnO) films. They found that the deposited thin films had a hexagonal wurtzite structure with optical transmittance (77%−92%) in the visible. Increasing Cu concentration decreased the crystallite size and the surface roughness of the films and increased the optical gap of prepared films.

To study the optical properties and the chemical structure of copper doped zinc oxide thin films. Caglar et al [4] employed sol‑gel spin coating technique. They investigated bonding states and the impact of the copper combination of the film's composition and morphological characteristics of zinc oxide films. They found that the copper dopant altered the structure and optical characteristics of the zinc oxide films because copper ions were oxidized in the zinc

oxide composition and replaced into the zinc oxide lattice at the Zn^{2+} place. They determined the surface roughness increases with doping.

Al-Khanbashi et al [5] used the sol–gel dip-coating technique to prepare (Cu: ZnO) thin films with different concentrations of copper in the range 0–5 wt%. They studied the optical properties and the structure of thin films. They concluded that grains without voids were distributed homogeneously on the surface of the films, which confirmed the (Cu: ZnO) films had a hexagonal wurtzite structure. The increasing concentration of Cu leads to reduce the energy of band gap.

1.5.3 SPRAY PYROLYSIS TECHNIQUE

Tarwal et al [30] investigated the impact of copper on the structure and visual characteristics of ZnO thin films, which were prepared by spray pyrolysis. They observed that the copper concentration increased in the thin films lead to a reduction in the optical band gap energy of the films and noticed that thin films had hexagonal crystal structure due to their polycrystalline nature.

Mani et al [31] used spray pyrolysis technique to prepare nanostructured un-doped and copper-doped zinc oxide thin films. They characterized the construction and optical characteristics of the thin films in order to confirm the polycrystalline nature of the thin films with hexagonal wurtzite structure. They found that increase in copper dopant concentration reduced the optical band gap value from (3.12 to 2.72) eV and lead to a decrease in the grain size in the films.

1.5.4 OTHER TECHNIQUES

Mhamdi et al [32] used chemical spray technique to deposit (Cu: ZnO) thin films at various concentration (1–3%) on a glass substrate at 460 ˚C. They studied the frequency relaxation

phenomenon, optical measurements and structural topography properties of deposited thin films. They revealed that copper ions take up alternative positions without change to the hexagonal structure. They investigated that the deposited films show a direct band gap relative to high absorption coefficient ($\alpha > 10^4$ cm^{-1}) of the thin films.

The structure and the magnetic properties of (ZnO: Cu) films were reported by Qing Ma et al [25] using pulsed-laser ablation under different conditions of Cu content in the films. They reported that (ZnO: Cu) films had a hexagonal wurtzite structure. The copper ions in theses samples at most were Cu^{2+}. There were no detectable oxygen vacancies in the (ZnO: Cu) films.

Malik et al [33] deposited Cu-doped ZnO films using pulsed laser deposition on quartz substrates. They characterized the crystalline structure and the exterior surface of the deposited thin films. They found that films had strongly preferred c-axis direction and Cu ions doping in ZnO lattice didn't alter the hexagonal wurtzite structure in copper-doped zinc oxide films.

Kumar et al [34] used scanning probe microscopy (SPM) to study the bipolar charge phenomenon in copper and cobalt co-doped zinc oxide (ZnO) film. A pulsed laser deposition (PLD) technique was used to prepare un-doped ZnO samples. They characterized the crystal structure of thin films and observed that Cu and Co co-doped ZnO thin film can store the bipolar charge. They found that positive charges in ZnO stabilized by doping copper and the negative charges stability improved by doping Co.

Alivov et al [35] created thin films by using thermal diffusion to doped copper with high-quality ZnO single-crystal films. They studied their luminescent properties. They concluded that the oxygen vacancies were responsible for the green luminescence band in this material

and the copper impurity is responsible for the formation of the green band in the luminescence spectrum of zinc oxide.

1.6 SCOPE OF WORK

A lot of studies have been done so far in order to investigate the copper-doped zinc oxide thin films under various conditions via different deposition techniques. The aim of this work is to investigate the effect of Cu doping with different concentrations on the structural, morphological, chemical, electrical and optical characteristics of zinc oxide thin films. All the films were deposited by magnetron co-sputtering technique with high purity targets of Cu and ZnO. In addition to that, the sample under power 18 W was annealed at fixed temperature with an oxygen environment. The structural characteristics, surface morphology and the chemical composition of the resulting films were investigated. Moreover, the optical properties of the resulting films were determined.

CHAPTER 2

EXPERIMENTAL TECHNIQUE

In this chapter, I will provide a description of the sputtering technique. This is followed by a description of the characterization techniques used to analyze the properties of thin films.

2.1 SPUTTERING TECHNIQUE

There are different methods to deposit materials onto a surface (substrate) to form a thin film. Preparation of thin films by physical vapor deposition (PVD) has been used in many industrial sectors and a wide field of coating applications [36]. Sputtering is an important physical vapor deposition (PVD) technique [37] that is used to deposit thin films onto substrates [38]. Sputtering is the physical ejection of atoms from solid or liquid targets because of the energetic impact of bombarding particles [37]. There are different methods to enhance this process. One common way to do this is by using magnetrons [38]. Figure 2.1 shows a schematic diagram of a sputtering system. Magnetron sputtering is widely applied both in industrial processes and in advanced material development or treatment, and now it is considered as the most effective process for the deposition of metals, alloys, ceramic, and polymer thin films onto a wide range of substrate materials [39, 36].

Plasma is the fourth state of matter, with the other three states of the matter being solid, liquid and gas. Plasma is a distinguished state of matter containing a large number of electrically charged particles. Naturally, each atom has an equal number of electrons and protons where the protons in the nucleus are surrounded by an equal number of electrons so that each atom is

electrically "neutral". A gas becomes "plasma" when a significant number of atoms release some of their electrons and become ionized [40]. To create a plasma, a discharge gas is introduced. The gas is often inert, to avoid unwanted reactions with the target material. The most common gas used in sputtering processes is argon (Ar). Neutral argon atoms are introduced into a vacuum chamber at a low pressure which is required to maintain high ion energies and to prevent too many atom-gas collisions after ejection from the target [41]. An electric field is applied between the sputtering target (cathode) and an anode. Often, the chamber wall and the substrates are used as the anode in the system. At room temperature, the gas will contain a small fraction of ions and some free electrons. The electric field ionizes argon atoms and creates a plasma (glow discharge). These argon ions are accelerated towards the target and argon electrons are accelerated to the anode substrate [40]. The strong collision of these ions onto the target ejects target ions and negative particles into space. These ejected particles are condensed on the film and bind each other at the molecular level so that the ejected electrons form a tightly bound layer [41]. Usually, a parallel magnetic field is superposed on the glow discharge. Electrons in the plasma show cycloid motion. The magnetic field is oriented so as to drift the paths of electrons to form closed loops. This causes an increased rate of collision between the electrons and the sputtering gas molecules. The magnetic field causes the plasma density to increase, causing an increase in the sputtering rate and efficiency of the sputtering process [37].

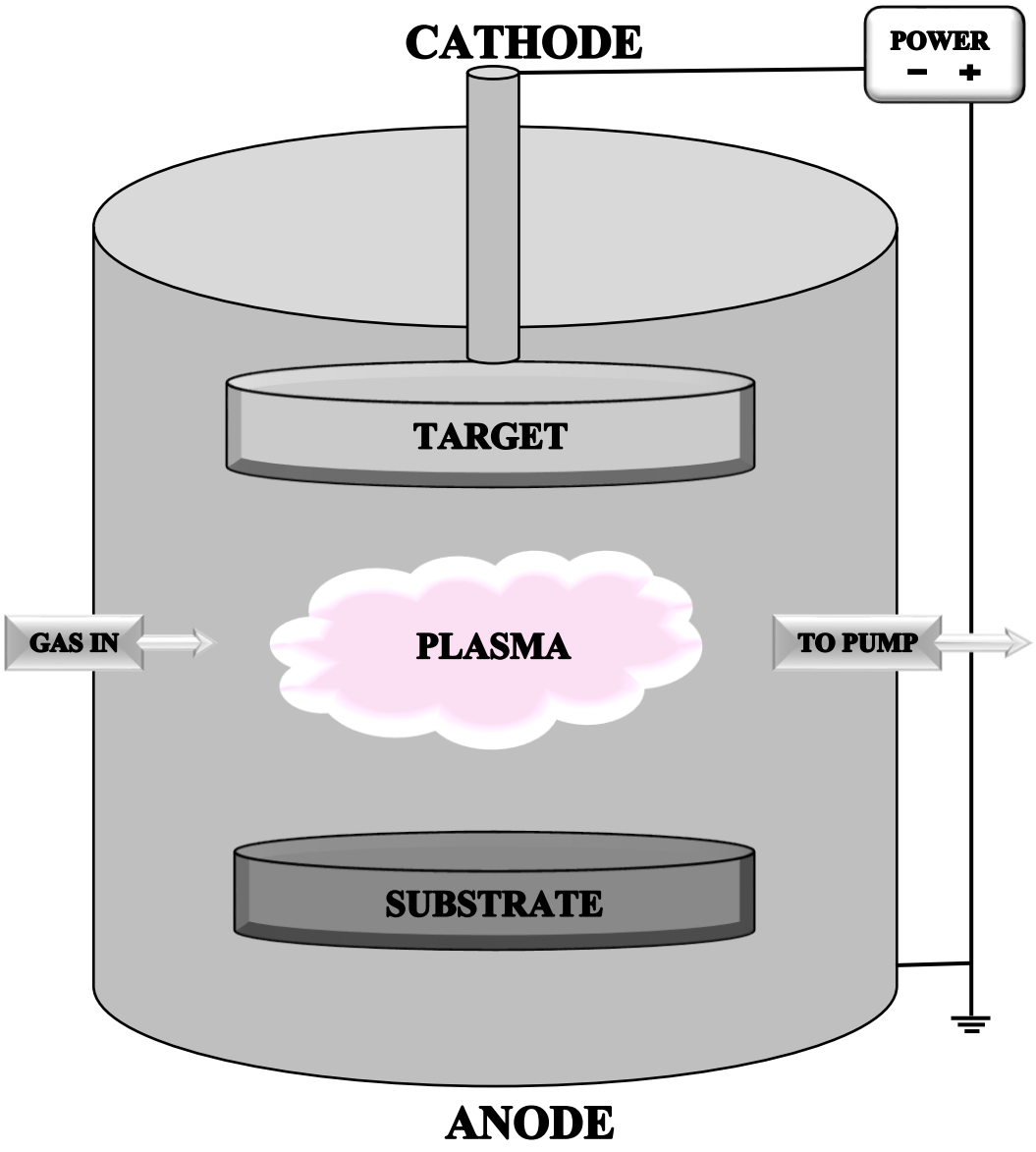

Figure 2.1. Schematic diagram of a sputtering system

2.1.1 DIRECT CURRENT MAGNETRON SPUTTERING

Direct current magnetron sputtering is the simplest and least expensive way to deposit thin films using a DC power supply. The fundamentals of this technique can be described in terms of a glow discharge between two plates forming a capacitor. The target made out of the precursor material (cathode) and the substrates for growing the thin film (anode) are facing each other and are attached to the electrodes. An inert gas, usually argon, is introduced between the two electrodes to serve as a medium for initiating and maintaining the glow discharge. Electrons make collisions with the argon atoms, which cause them to ionize or reach a metastable state. The resulting positive ions (Ar^+) are subsequently accelerated to the target where they dislodge neutral atoms through momentum transfer. These atoms from the target also become part of the discharge and deposit on the substrate to form a thin film [42].

2.1.2 RADIO FREQUENCY MAGNETRON SPUTTERING

Radio frequency (RF) sputtering is mainly used to deposit non-conductive targets. In the case of insulators, after the ions strike the surface, their charge will remain localized and with the passage of time positive charge will build up on the target, making it unfeasible to further bombard the surface. This can be prevented by bombarding the insulator by both positive ions and electrons simultaneously. That is done by applying an RF potential to the target [38]. Typically RF frequencies are employed in the range from 5 to 30 MHz. However, for the most general frequency used for RF sputtering (13.56 MHz), ions and electrons have vastly different mobilities in the fluctuating field. This means they physically move different distances during each half cycle [41]. The RF potential provides sufficient energy to the electrons oscillating in the alternating field to cause ionizing collisions, and a self-sustained discharge is maintained. As electrons have higher mobility compared to ions, more electrons will reach the insulating

target surface during the positive half cycle than the positive ions during the negative half cycle. Hence the target will be self-biased negatively. This repels the electrons from the vicinity of the target and forms a sheath enriched in positive ions in front the target surface. These ions bombard the target and sputtering are achieved [43]. The most important difference between RF and DC systems is that the deposition rate for RF sputtering is only half the deposition rate for DC sputtering when the same power is applied; this makes RF sputtering not an attractive candidate for the large-scale industrial application.

2.1.3 MAGNETRON CONFOCAL SPUTTERING

Confocal sputtering is the important technique of arrangement magnetrons during a vacuum chamber. Confocal sputtering also known as co-sputtering allows the user to make a film of two or more materials at once. These multiple materials can be applied onto the substrate without breaking the vacuum of the chamber. In a confocal sputtering arrangement, the cathodes are concentrated on a central area of the substrate. Table rotation through sputtering allows co-deposition on the substrate. The continuous rotation permits the substrate exposure to the cathodes and creates an excellent coating uniformity. The co-sputtering technique provides many advantages to the user and adds flexibility to the system. It increases the yield of the sputtered material, improves the film uniformity and shortens the time for the creation of the films by using multiple targets simultaneously. Co-sputtering is highly recommended for Today's cutting edge research and development systems [44]. A diagram of the co-sputtering system used in this work is shown in figure 2.2.

2.1.4 ADVANTAGES OF MAGNETRON SPUTTERING

In recent years, there has been an increasing interest in the growth of ZnO thin films by magnetron sputtering. Magnetron sputtering technique has some advantages compared to the

other methods such as: simple physical process, flexibility to adapt to individual requirements, a large area deposition [45], easier controllability of the deposition parameters, high deposition rates [46], high-purity films, ability to coat heat-sensitive substrates, ease of automation, excellent uniformity on large-area substrates [41], low substrate temperature, good adhesion, and high melting point materials can be deposited and well suited for alloys and compounds. It is clear that sputtering is a very powerful technique which can be used in a wide range of applications [41].

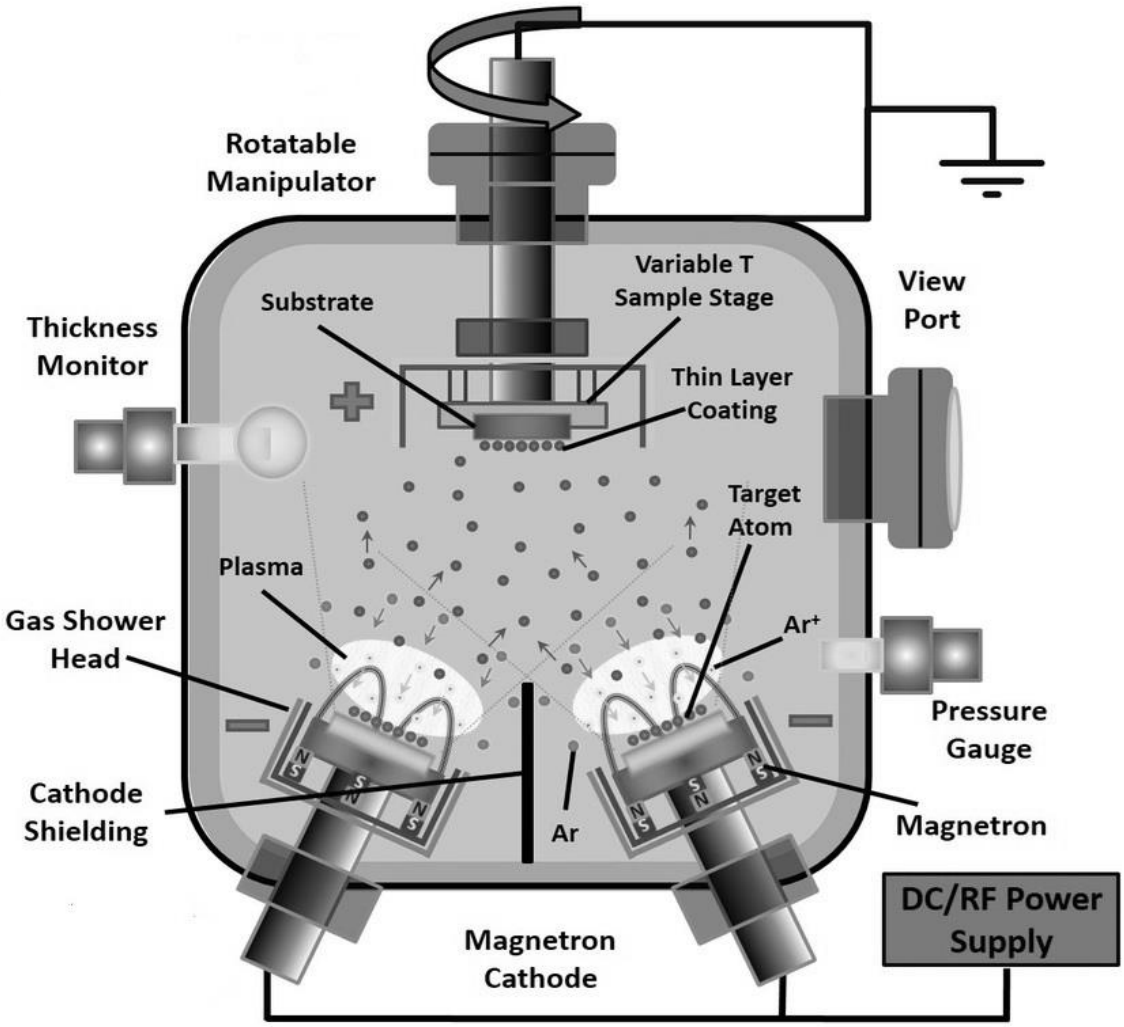

Figure 2.2. Schematic diagram of confocal sputtering system

2.2 THIN FILM DEPOSITION AND PROCESSING

Thin film deposition was carried out by magnetron co-sputtering technique. I prepared (Cu: ZnO) thin films via magnetron co-sputtering of zinc oxide target and copper target. Cu target with a purity of (99.99%) was sputtered by a direct current (DC) power supply and ZnO target with a purity of (99.99%) was sputtered by a radio frequency (RF) power supply. The distance between the targets and the substrates was 11cm. Two shutters were used in front of the Cu and ZnO targets respectively, to avoid excessive doping. The deposition chamber was initially pumped down to a base pressure of 8×10^{-6} mbar. The flow rate of introduced argon gas (99.99% purity) was 10 sccm to maintain a constant chamber pressure of 1.9×10^{-2} mbar. Prior to deposition, the substrates were cleaned by methanol and then dried using compressed argon. The substrates were rotating during the deposition at a speed of 6 rpm. The atoms of targets were deposited on substrates for two hours. The substrate temperature was kept at room temperature. The sputtering power of zinc oxide target was kept at 100W, and the sputtering power of copper was set to 10, 12, 14, 16, and 18 W to obtain different doping content. The films were deposited on fused silica substrates. Crystallinity characterization was performed by X-ray diffraction (XRD). Surface morphology was examined by atomic force microscopy (AFM), the chemical composition was investigated by X-ray fluorescence (XRF), optical measurements were determined using a spectrophotometry, and electrical resistivity was determined using the high current source measure unit. Also, thin films were deposited on tantalum substrates for X-ray photoelectron spectroscopy (XPS).

2.3 CHARACTERIZATION TECHNIQUES

Various characterization techniques were used to examine the characteristics of the thin films. Several of these techniques are:

2.3.1 SURFACE MORPHOLOGICAL ANALYSIS

Atomic force microscopy (AFM) is a high-resolution scanning probe microscopy technique that is valuable for studying microstructured and nanostructured surfaces. Also, the topography properties of the surface of a sample were investigated by this technique. A sharp probe of the order of nanometers attached to a spring loaded cantilever is used for scanning the surface of a specimen. Light from a laser shining on the cantilever is detected by a photodiode and the resultant signal generated is interpreted by specialist electronics. The tip (probe) is generally made from a ceramic or sometimes made from a semiconducting material, but recently the probes have been made from flexible and strong nanotubes that are cylindrical carbon nanotubes. The tip radius is typically between 5-15 nm. The working principle of atomic force microscopy (AFM) is based on scanning of the sharp tip across the specimen area. When the tip approaches the sample surface during a few angstroms, forces between the atoms of the specimen surface and the tip are converted into a deflection of the cantilever. Atomic force microscopy involves some forces which are van deer Waals forces, electrostatic forces, magnetic forces, and bonding forces. The magnitude of the deflection depends on the distance between the tip and specimen surface. The deflection is measured by using a laser beam which is reflected from the backside of the cantilever onto a distant photo-detector. A schematic diagram of an atomic force microscope is shown in figure 2.3. The surface morphology of our films was investigated by Veeco Innova diSPM. The surface of the sample was probed with a

10 nm radius silicon tip oscillating at its resonant frequency of 300 kHz. The scan area was $2\times2\ \mu m^2$, and the scan rate was 2 Hz.

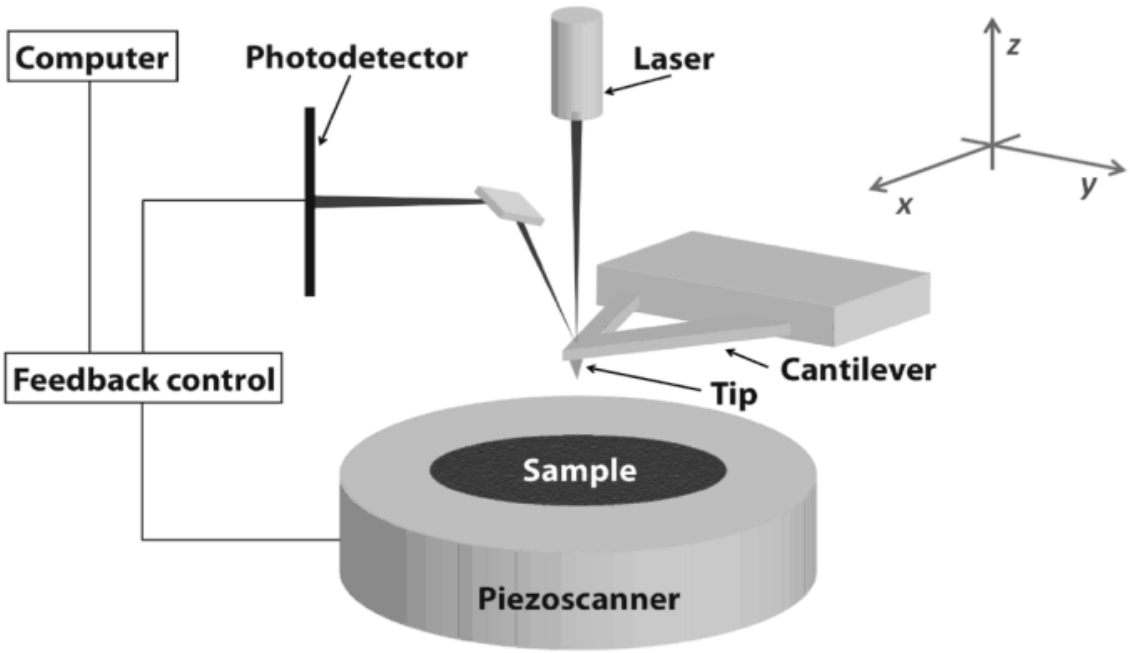

Figure 2.3. A schematic diagram of an atomic force microscope

2.3.2 STRUCTURE ANALYSIS

X-rays are electromagnetic waves with a short wavelength, high energy and high frequency inhabiting in the area between gamma rays and ultraviolet radiation [37]. X-ray diffraction (XRD) is an indispensable non-destructive technique for the qualitative and quantitative analysis of a wide range of materials. It is used to characterize the crystal composition, grain size and preferred orientation in polycrystalline or powdered solid specimens. X-ray diffraction is based on constructive interference of monochromatic X-rays. X-rays are generated by a cathode ray tube which operates by the acceleration of electrons to high energy. These rays are filtered to produce monochromatic radiation which is collimated to concentrate these rays then directed these rays onto the specimen [47]. It can investigate the structure of matter at the molecular level and is commonly used for the determination of positions of atoms in a crystalline structure. When an X-ray impinges onto a solid specimen, there is some portion of the beam that is scattered by the atoms [37]. When the beam is incident at an angle θ onto the specimen, constructive interference of the scattered rays may occur and a peak in intensity occurs at the same angle with the plane [47]. The diffraction of X-rays by specimens is described by Bragg's law.

$$n\lambda = 2d_{hlk}sin\theta \qquad (2.1)$$

where n is an integer, λ is the wavelength of electromagnetic radiation, θ is the diffraction angle of the incident radiation, and (d_{hlk}) is the lattice spacing between the two atomic planes in a crystalline specimen. A schematic diagram showing the geometry of Bragg's law is given in figure 2.4. The structure of our films was investigated by XRD using Burker D8 Advance X-ray diffractometer. The 2θ step was 0.02^{o} and the step acquisition time was 1s.

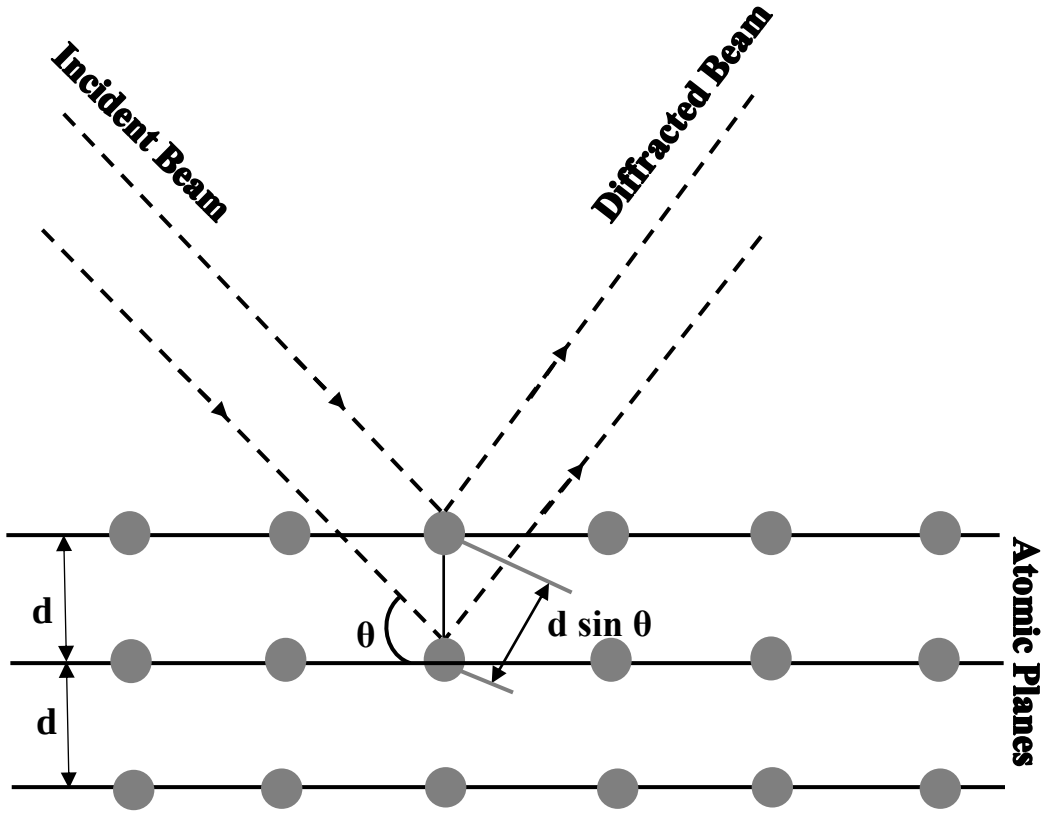

Figure 2.4. Schematic diagram of Bragg's law

2.3.3 CHEMICAL ANALYSIS

X-ray photoelectron spectroscopy (XPS) is one of the most powerful and common chemical analysis techniques [48]. It is a non-destructive technique for studying the electronic structure of atoms, molecules, and solids specimen. Plenty of the properties of solid materials depends on the chemical composition of surfaces and interfaces in atomic dimension [49]. X-ray photoelectron spectroscopy is used for the acquisition of high-resolution spectra in binding energy regions for the chemical state of the samples. With XPS it is possible to probe the shell structure of atoms and the electronic band structure of solids and understand the electronic structure of matter. X-ray photoelectron spectroscopy (XPS) relies on the photoelectric impact. Each atom has core electrons with a distinct binding energy that is equal to the ionization energy of that electron. A sample placed in an ultra-high vacuum is irradiated with photons of energy (hv) [50]. When an X-ray beam directs to the specimen surface, the energy of the X-ray photon is absorbed completely by the core electron of an atom. If the energy of the photon (hv) is greater than the binding energy (E_b) of the electron and the electron has enough energy to overcome the work function (ϕ) of the solid then the core electron will escape from the atom. Photoelectron is the emitted electron with a kinetic energy of E_k. The binding energy of the core electron is given by the Einstein relationship:

$$hv = E_k + E_b + \phi \tag{2.2}$$

$$E_k = hv - E_b - \phi \tag{2.3}$$

where hv is incident photon energy, h is the plank's constant (6.62×10^{-34} J.s), v is the frequency of the photon, E_b is the binding energy of an electron, ϕ is the work function which is the minimum energy needed to remove an electron from a solid. A schematic diagram of the basic principle of XPS is shown in figure 2.5. Whilst X-ray photoelectron spectroscopy is a

surface sensitive technique, a depth profile of the specimen in terms of X-ray photoelectron spectroscopy quantities could be obtained from the surface or interface of the samples. Depth profile analysis is a versatile method to analyze thin films to get the in-depth distribution of the elemental composition at surfaces and at interfaces of thin films. Depth profiling is used in many laboratories due to its installation of an ion gun in a surface analysis chamber and interpretation of the raw data, which consist of an elemental intensity versus the sputtering time. An ion gun is utilized to etch material for a period of time before being turned off while XPS spectra are acquired. Each ion gun etch cycle exposes a new surfaces of the samples and the X-ray photoelectron spectroscopy provides means of analyzing the composition of these surfaces in the thin films. The actual depth for each X-ray photoelectron spectroscopy analysis is dependent on the etch-rate of the ion-gun, which in turn relies on the material being etched at any given depth [49]. The XPS of our films was investigated in a Thermo Scientific Escalab 250Xi spectrometer.

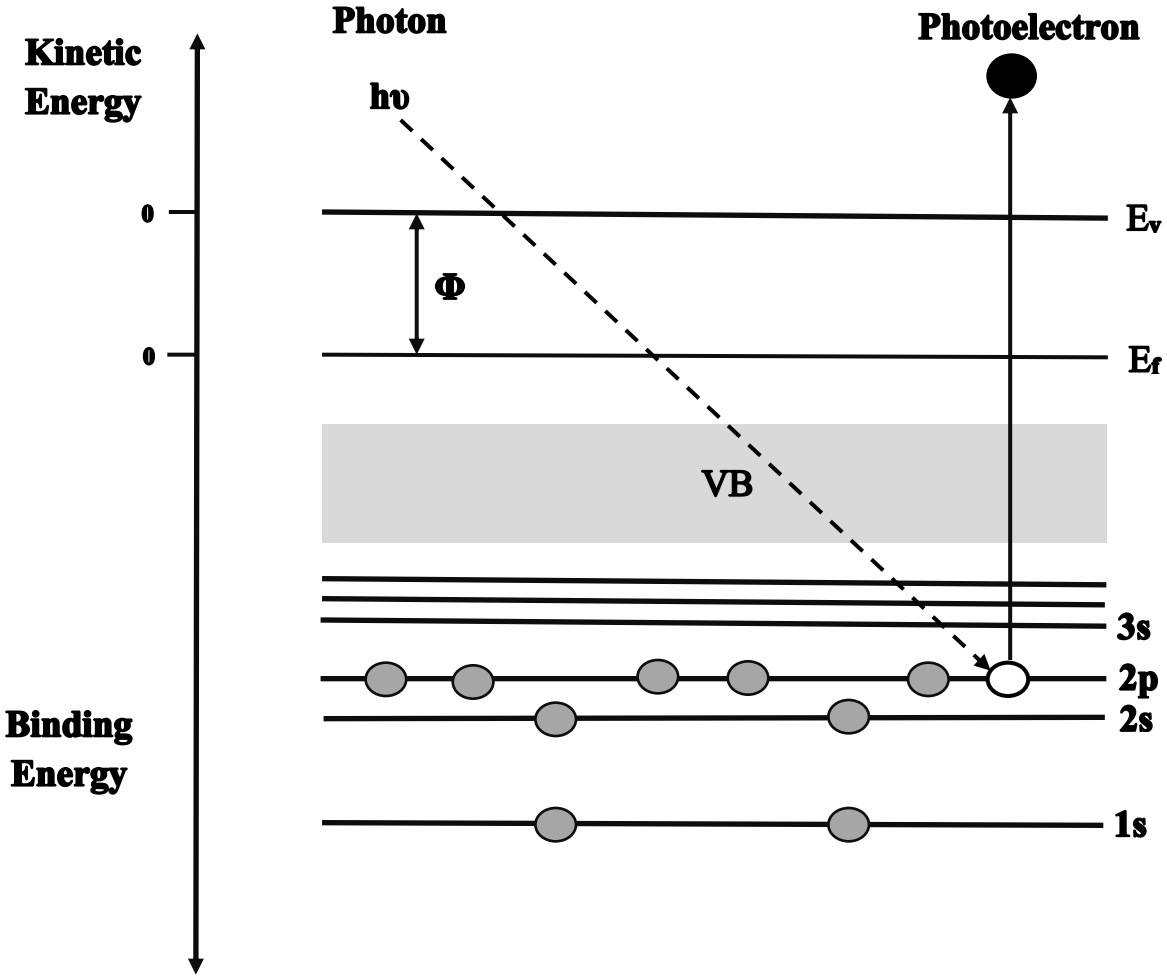

Figure 2.5. Schematic diagram of the basic principle of XPS

2.3.4 CHEMICAL COMPOSITION

X-ray fluorescence is the emission of distinct X-rays from a material that has been excited by bombarding with high-energy photons [51]. X-Ray Fluorescence is a powerful technique for chemical analysis in all kinds of materials, which is considered as one of the most widespread methods used in industrial and research applications for materials characterization. When high energy photons are absorbed by atoms, inner shell electrons are ejected from the atom, becoming “photoelectrons”. These electrons leave the atoms in an excited state, with a vacancy in the inner shell. Outer shell electrons then fall into the vacancy, emitting photons with an energy that is equal to the energy difference in binding energy of the two shells [51]. A schematic diagram showing the basic principle of XRF is given in figure 2.6. The concentration of copper in of our films was investigated using a Spectro Xepos EDX XRF2 spectrometer.

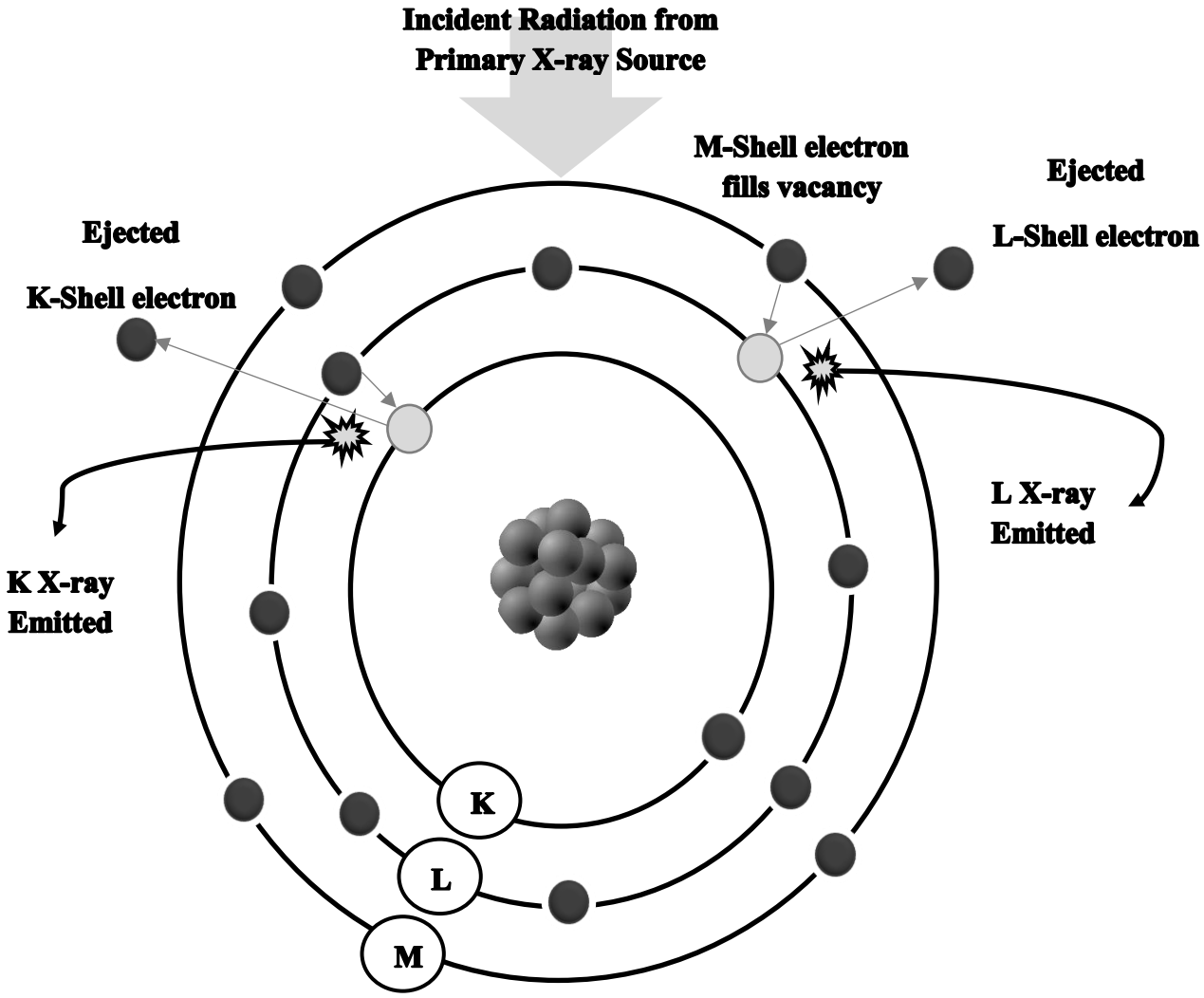

Figure 2.6. Schematic diagram of the basic principle of X-Ray fluorescence

2.3.5 OPTICAL MEASUREMENTS

The optical properties of a material such as absorption coefficient, refractive index, and band gap can be extracted from optical measurements. The optical measurements of a material deposited as thin film are demonstrated in a schematic diagram in figure 2.7. The interactions between the radiation and the thin film take four ways part of the radiation is absorbed by the thin film, a fraction of the radiation is transmitted through the film, some of the radiation is reflected from the surface of the film, and part of the radiation is scattered from the film. In general, all contributions are given by the following equation:

$$A + R + S + T = 1 \qquad (2.4)$$

Where A is absorbed radiation, R is reflected radiation, S is scattered radiation and T are transmitted radiation. The optical properties of our films were determined by measuring the normal incidence transmittance of the films over the wavelength range of 300-800 nm using a Jasco V-570 spectrophotometer.

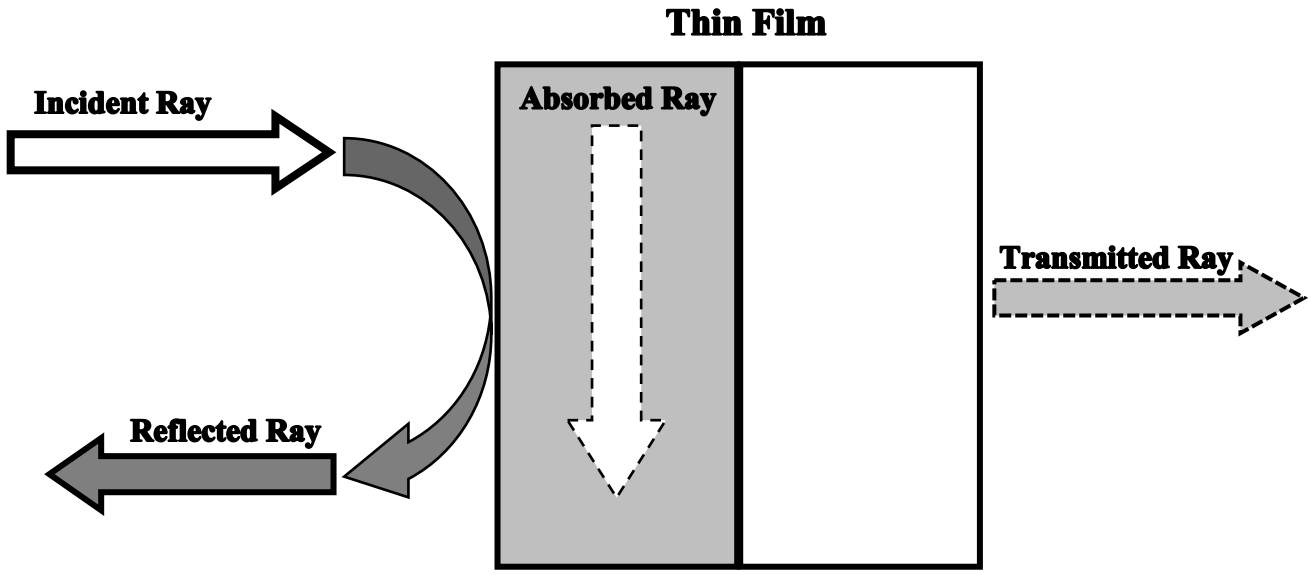

Figure 2.7. Schematic diagram of optical measurements of thin film

CHAPTER 3

STRUCTURAL AND CHEMICAL CHARACTERISTICS

3.1 STRUCTURAL PROPERTIES

The thickness of the films was determined from the interference fringes in the transmittance spectra (see chapter 4), and their values are given in table 3.1, which depicts a steady increase in thickness as the DC sputtering power increased. This is due to the deposition of more sputtered species as the DC power increases. Zinc oxide (ZnO) crystallizes in the hexagonal wurtzite structure. The bonding of zinc oxide is largely ionic, with the corresponding radii of 0.140 nm for O^{-2} and 0.074 nm for Zn^{+2}. The valance band of zinc oxide is formed basically from the 2p levels of O^{-2}, and the conduction band is formed essentially from the 4s levels of Zn^{+2}. Doping zinc oxide with different concentrations of copper may change the structural properties of zinc oxide thin films [7]. The structural characteristics of the copper doped zinc oxide thin films with different Cu concentration were investigated by X-ray diffraction (XRD). Figure 3.1 shows the XRD patterns of pure, and copper-doped zinc oxide thin films. As can be seen from figure 3.1- a for pure zinc oxide, the films exhibited a single peak corresponding to the (002) reflection of the hexagonal wurtzite structure, indicating strong orientation along the c-axis. Figure 3.1- b shows the XRD pattern of a doped film with a DC power of 10 W applied to the copper target. The intensity of the (002) peak was enhanced, and an additional peak along the (101) direction appeared. No peaks corresponding to Cu or its oxides were observed, which may be due to the replacement of Zn atoms by Cu atoms at the hexagonal

lattice or the segregation of Cu atoms into interstitial sites [52, 53]. The enhancement of the crystallinity could be ascribed to the creation of new nucleation sites due to Cu doping [30]. With further increase in the DC power (i.e higher dopant concentration), the crystallinity deteriorated drastically, and the films depicted an amorphous structure as shown in figure 3.2. The degradation of the crystallinity at higher dopant concentrations may be attributed to several factors: (i) saturation of the new nucleation center [30] and transformation of the nucleation from homogeneous to heterogeneous [53], (ii) collision of ad-atoms with the films [20], and (iii) the smaller ionic radius of copper compared to that of zinc [52, 31] which causes deformation of the hexagonal lattice as the dopant concentration increases [54]. Previous reports indicated the presence of an optimum copper dopant concentration beyond which crystallinity starts to deteriorate [52, 53, 30]. The optimum concentration is critically dependent on the deposition technique.

Table 3.1. Physical properties of the films as functions of the DC power applied to the Cu target

Property	DC Power (W)					
	0	10	12	14	16	18
d (nm)	302	487	527	549	600	711
R_{rms} (nm)	7.80	10.02	0.92	0.60	0.58	1.53
Grain size (nm)	30.3	37.0	43.0	60.0	15.4	26.9

d = film thickness, R_{rms} = root-mean-square surface roughness

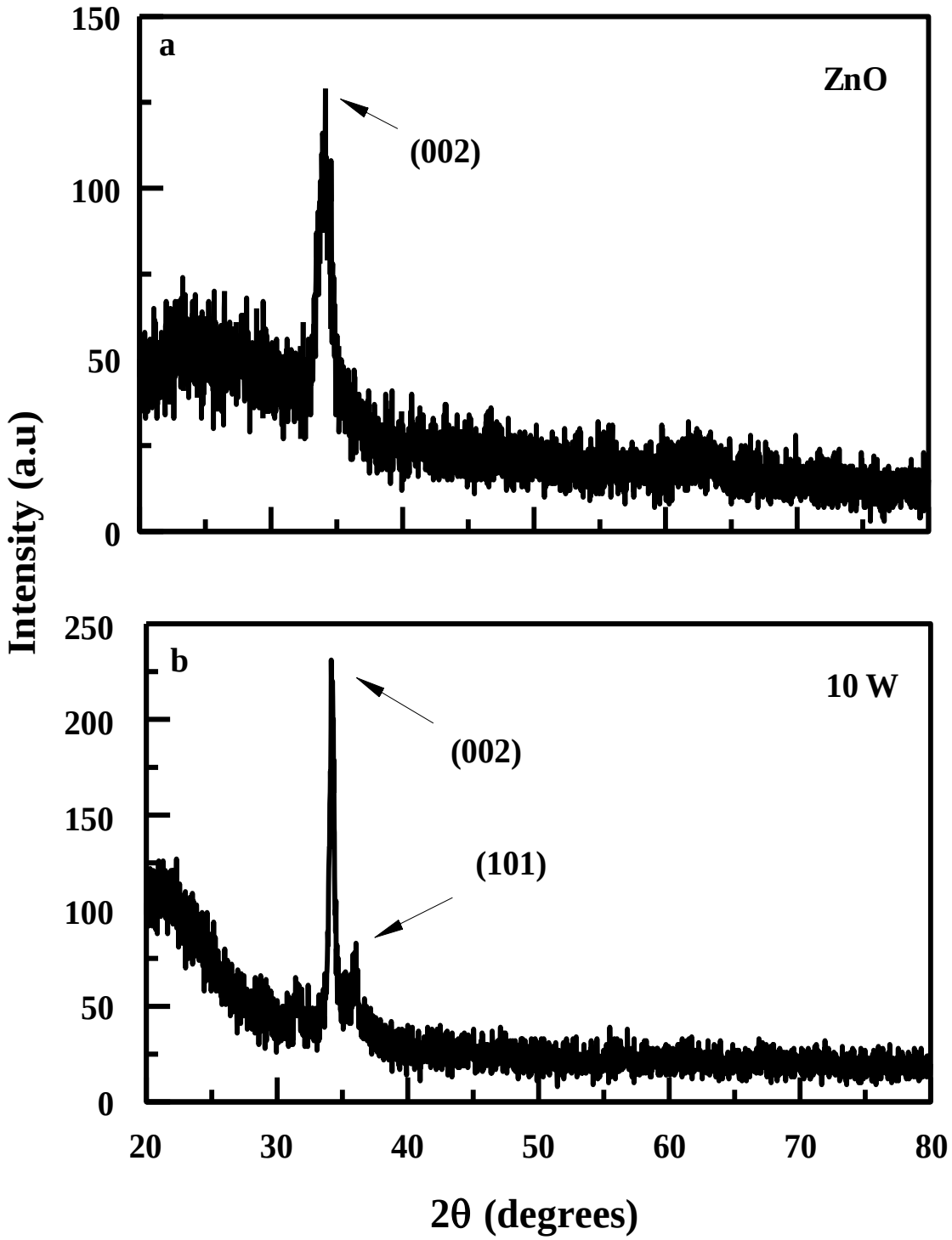

Figure 3.1. XRD patterns of the films. (a) Pure ZnO; (b)Copper-doped ZnO film deposited using co-sputtering with a 10-W DC power applied to the copper target.

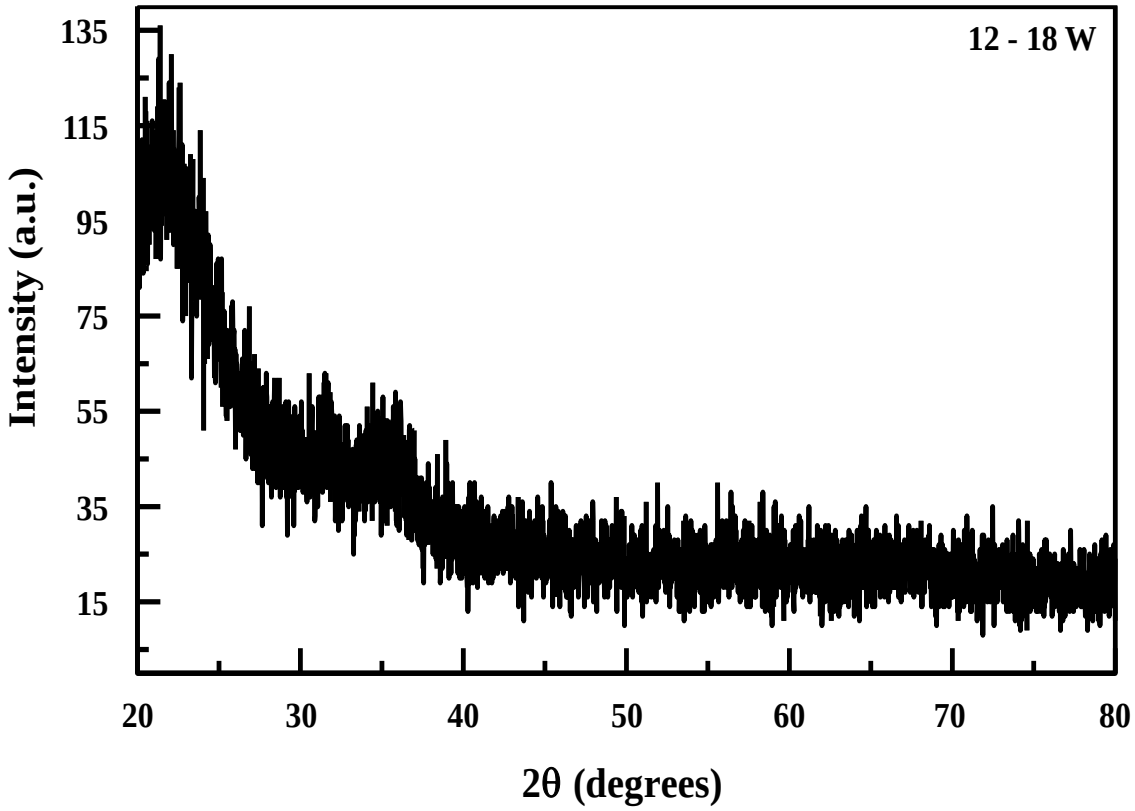

Figure 3.2. XRD patterns of copper-doped ZnO films deposited using co-sputtering with DC powers of 12 – 18 W applied to the copper target.

3.2 MORPHOLOGICAL PROPERTIES

Atomic force microscopy (AFM) was used to measure the surface morphology of pure zinc oxide and copper doped zinc oxide thin films. It is used to estimate the surface root-mean-square roughness (R_{rms}) and the lateral (surface) grain size. Typical three-dimensional and two-dimensional AFM images are shown in figures 3.3 and 3.4, respectively. They depict a columnar microstructure of films surfaces. The surface roughness and grain size values are listed in table 3.1. The morphology of undoped zinc oxide films was characterized by regular grains with a grain size value of 30.3 nm. Doping zinc oxide thin films up to 14 W increased the grain size without a significant change in morphology. Doping using a 16 W DC power resulted in significant reduction in grain size. Further doping at 18 W did not alter the morphology, although the grain size increased to 26.9 nm. On close inspection of the AFM images, it was observed that the root mean square (R_{rms}) surface roughness of the films decreased with an increase in Cu doping concentration, indicating that appropriate Cu doping content could decrease the surface roughness of zinc oxide thin films. This was due to the fluctuation of grain size which resulted in a decrease in surface roughness.

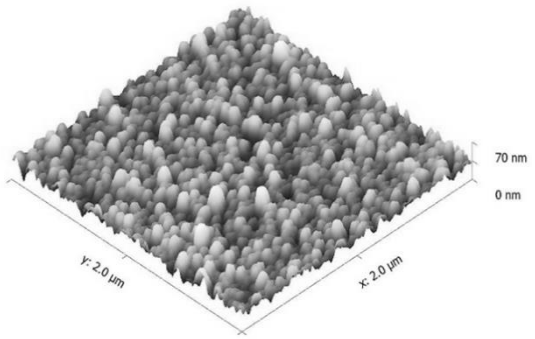

Pure ZnO

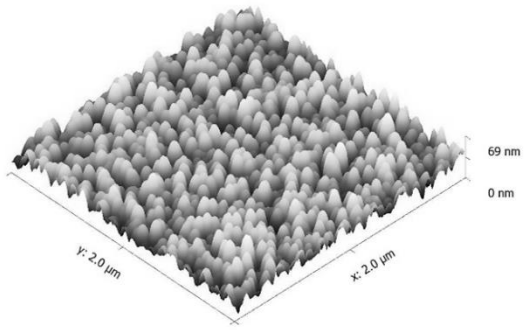

10 W

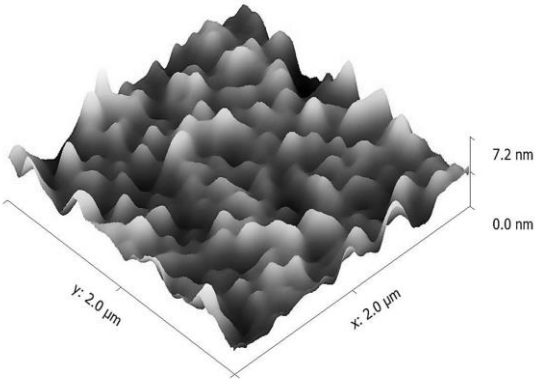

12 W

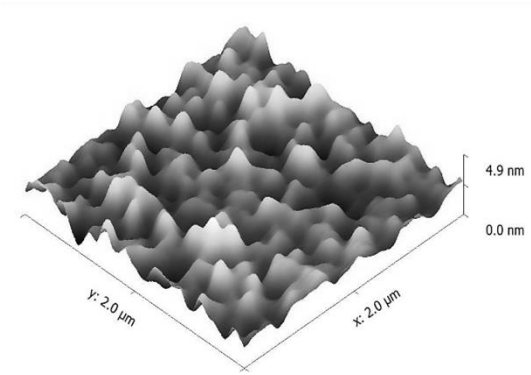

14 W

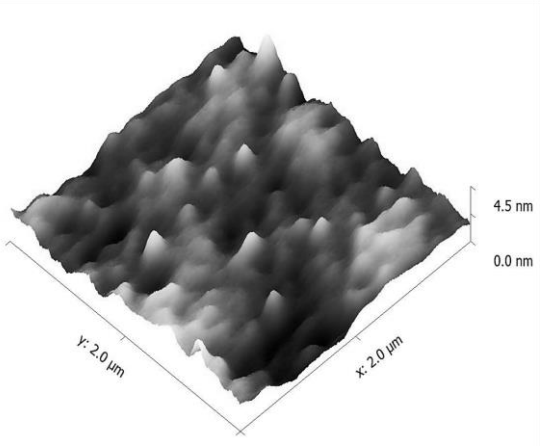

16 W

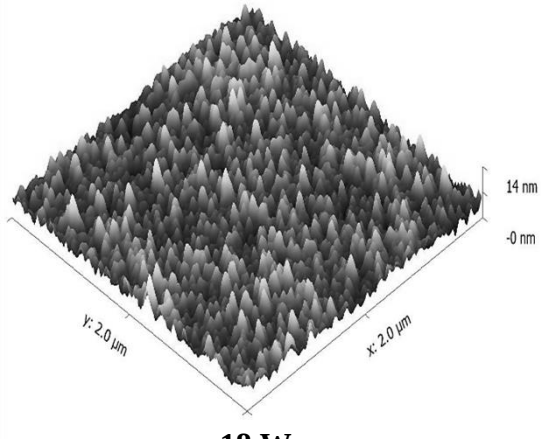

18 W

Figure 3.3. Three-dimensional AFM micrographs of Cu-doped ZnO films deposited using co-sputtering. The DC power applied to the Cu target is indicated on each image.

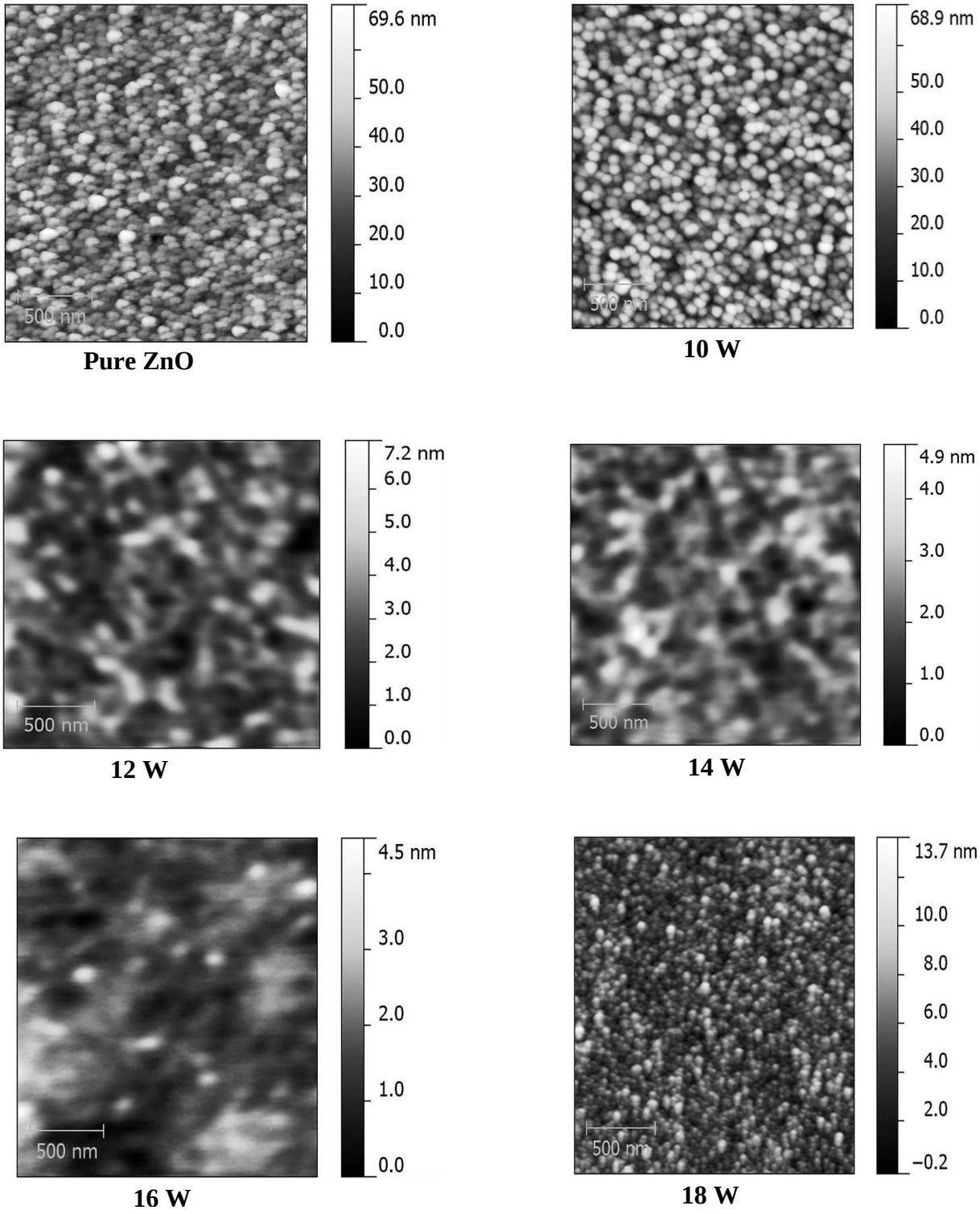

Figure 3.4. Two-dimensional AFM micrographs of Cu-doped ZnO films deposited using co-sputtering. The DC power applied to the Cu target is indicated on each image.

3.3 CHEMICAL ANALYSIS

X-ray photoelectron spectroscopy (XPS) is a surface technique that can investigate a few top layers of thin films. XPS technique a wealth of information about the surface chemistry of thin films. It provides information on the chemical oxidation state, chemical environment, valance band, and distribution of copper and zinc atoms in thin films [48]. The compositions and chemical properties of the pure and copper doped zinc oxide thin films were studied using XPS. A survey scan is a simple elemental identification achieved by recording low-resolution spectra over a broad binding energy range. A typical XPS wide survey scan is shown in figure 3.5. It reveals that the only elements present were the constituent elements (Zn, Cu, and O). In addition to the wide survey scans; detailed high-resolution spectra were obtained in the Zn 2p, Cu 2p, and O 1s core level regions. The Zn 2p core level spectrum consists of two sublevels ($2p_{1/2}$, and $2p_{3/2}$) due to spin-orbit splitting as shown in figure 3.6. The binding energy of the $2p_{3/2}$ peak in the undoped zinc oxide films and copper doped zinc oxide films was found to be 1021.8 ± 0.4 eV. This value is close to those reported in the literature [55], which conforms that Zn exists only as the oxidized state because no metallic Zn with a binding energy of about 1021.8 eV was observed [6]. The O 1s spectrum of pure zinc oxide thin films and copper doped zinc oxide thin films is usually asymmetric and has a complex structure due to the presence of several types of oxygen species [6]. The O 1s can be resolved into three component as shown in figure 3.7. The first component (A), which is at the low binding energy side corresponds to the Cu-O bond. The binding energy of this component was 529 ± 0.1 eV. The second component (B) in the O 1s spectrum is at a medium binding energy and corresponds to the Zn-O bond of crystal lattice oxygen. It is attributed to O^{-2} ions on wurtzite structure of hexagonal Zn^{+2} ion array. The binding energy of this component was 530.1 ± 0.1 eV. The third component

(C) in the O 1s spectrum is at the high binding energy side and corresponds to loosely bond surface oxygen species (such as CO^{-}_{3}, OH^{-}, adsorbed H_2O, and adsorbed O_2). The presence of this component may be attributed to the columnar structure of the surface of the films, which assists in the adsorption of these species. The binding energy of this component was 531.7 ± 0.2 eV. Similar to Zn, the Cu 2p core-level spectrum consists of two sublevels (Cu $2p_{3/2}$ and $2p_{1/2}$) due to spin-orbit splitting. The reported binding energy of metallic copper Cu^{0} for the $2p_{3/2}$ peak is 932.7 eV, and the binding energy of Cu in the copper oxides for $2p_{3/2}$ peak are 932.5 eV ($Cu^{+1} \leftrightarrow Cu_2O$), and 933.7 eV ($Cu^{+2} \leftrightarrow CuO$) [17, 56]. Evidently, it is very difficult to distinguish the cuprous oxide (Cu_2O) and metallic phase [17]. The CuO phase is further identified by the presence of a shake-up satellite structure at a binding energy of 93.0 eV [20]. A typical spectrum in the Cu 2p core-level region of our films is shown in figure 3.8. The binding energy of the Cu $2p_{3/2}$ peak was found to be 932.6 ± 0.1 eV. Thus, it can be concluded that copper exists in the films as a mixture of the Cu and Cu_2O phases. The close proximity of the binding energies of these two phases inhibits further resolution of the Cu $2p_{3/2}$ peak. The absence of the CuO phase is supported by the absence of the shake-up satellite. The presence of copper in an oxidized state could be due to the interaction of copper with the argon plasma [57], or the interaction with the oxygen-evolving from the ZnO target. The atomic concentration of the copper in the films (x) [Cu / (Cu + Zn)] was measured by X-ray fluorescence, and their values are listed in table 3.2. There was a monotonous increase in the concentration of copper as the DC sputtering power was increased. These values of atomic concentration reflect heavy copper doping in the deposited thin films.

The XPS depth profile analysis was used to investigate the Zn, Cu, and O concentrations across the thickness of the thin films as shown in figures 3.9 - 3.11, respectively. XPS depth profiling

shows that the elements where uniformly distributed throughout the thickness of the thin films. The increasing of thickness lead to increase in the etching time, which causes a shift in the graphs of Zn, Cu, and O respectively. Figure 3.11shows the oxygen concentration did not decrease because of the existence of oxygen from the atmosphere sitting on the surface of the substrate.

Table 3.2. Copper concentration (x) as a function of DC power

Property	DC Power (W)					
	0	10	12	14	16	18
x	--	0.263	0.309	0.361	0.419	0.511

x = copper atomic concentration

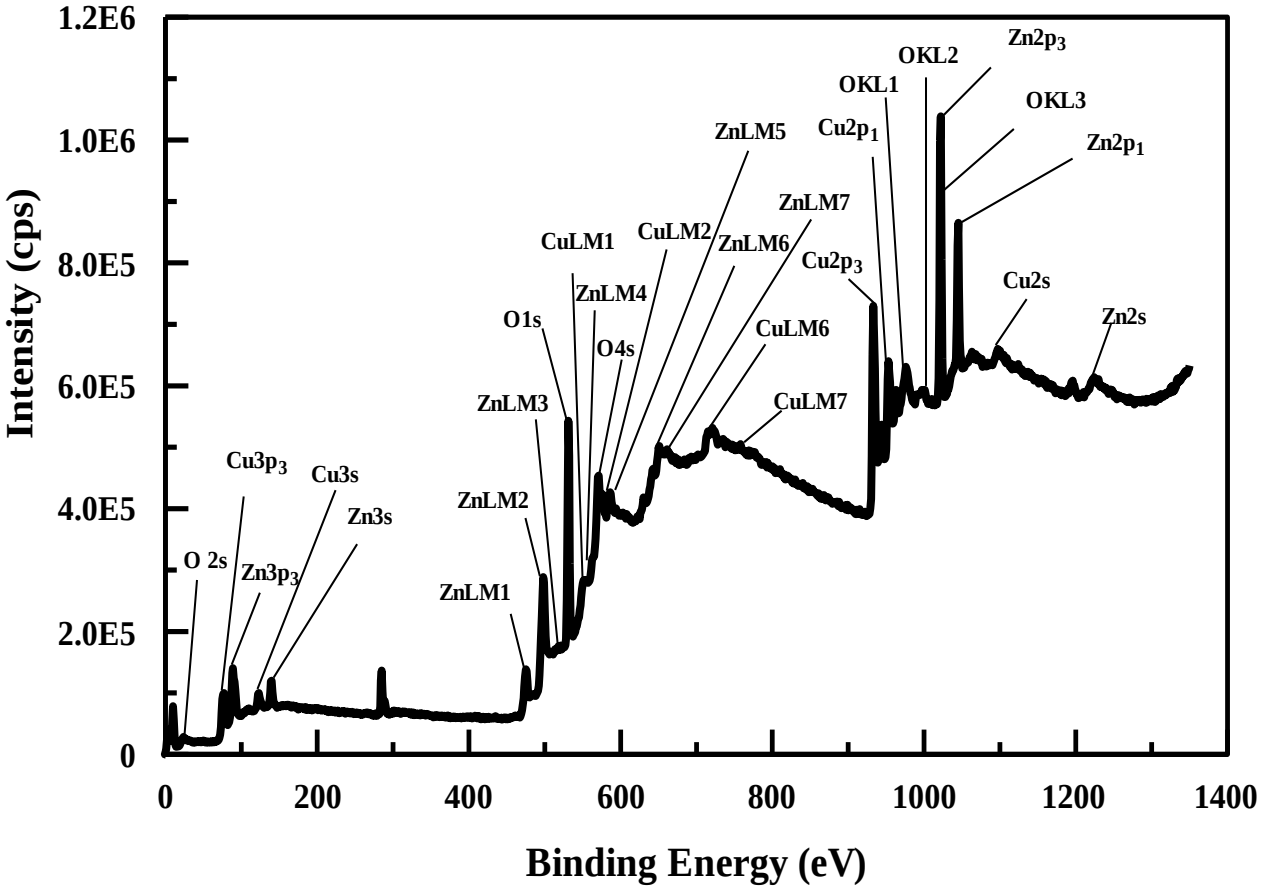

Figure 3.5. A typical XPS survey scan of a copper-doped ZnO film deposited using co-sputtering with an 18-W DC power, showing the main constituents of the film.

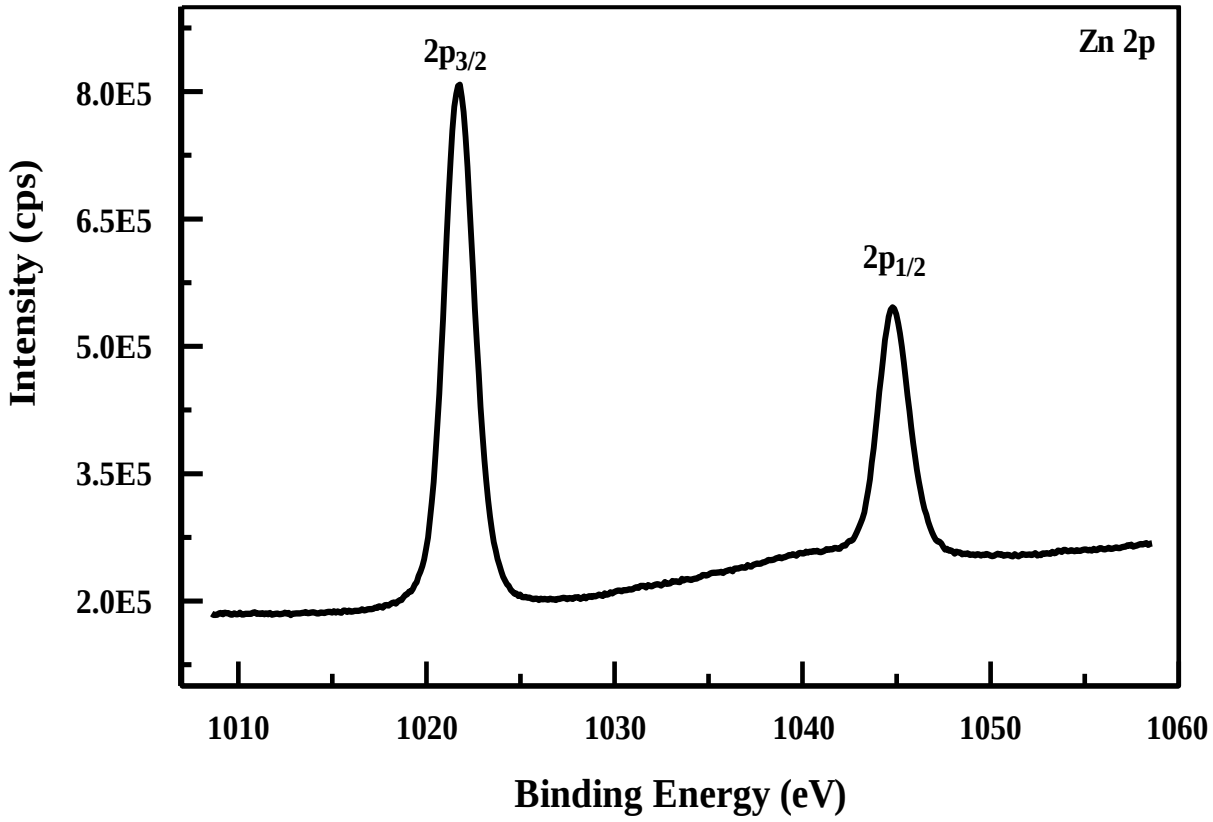

Figure 3.6. XPS spectra of a co-sputtered film using 18-W DC power applied to the copper target, showing the Zn 2p core-level spectrum.

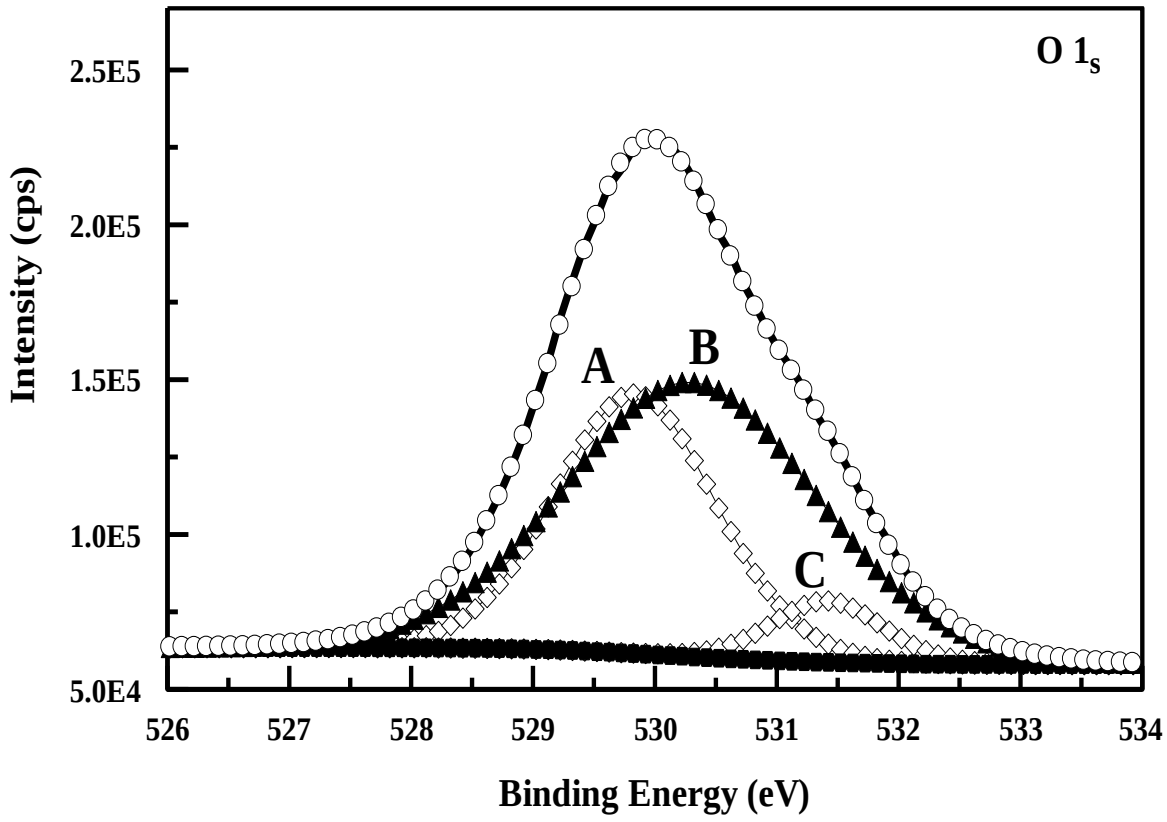

Figure 3.7. O1s XPS spectrum of a co-sputtered film using 18-W DC power applied to the copper target. The spectrum was resolved into its three components. The experimental spectrum is denoted by the open circles.

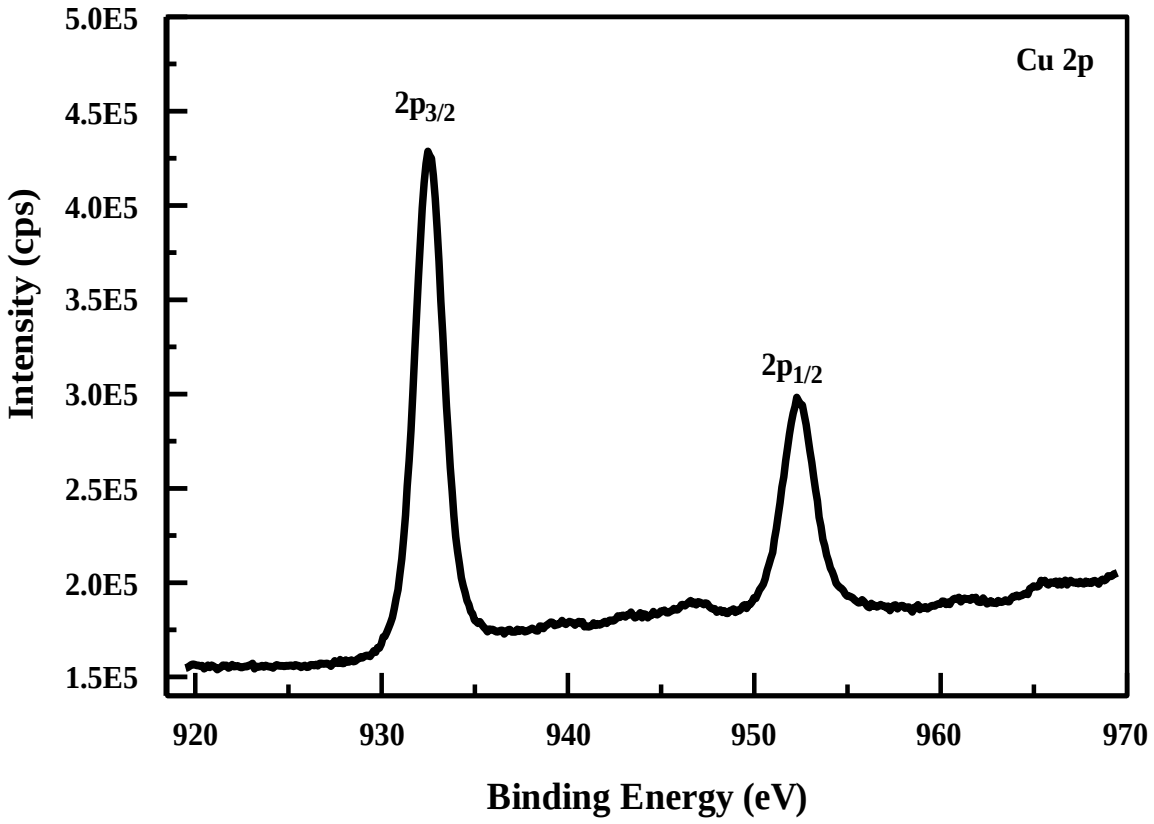

Figure 3.8. XPS spectra of a co-sputtered film using 18-W DC power applied to the copper target, showing the Cu 2p core-level spectrum.

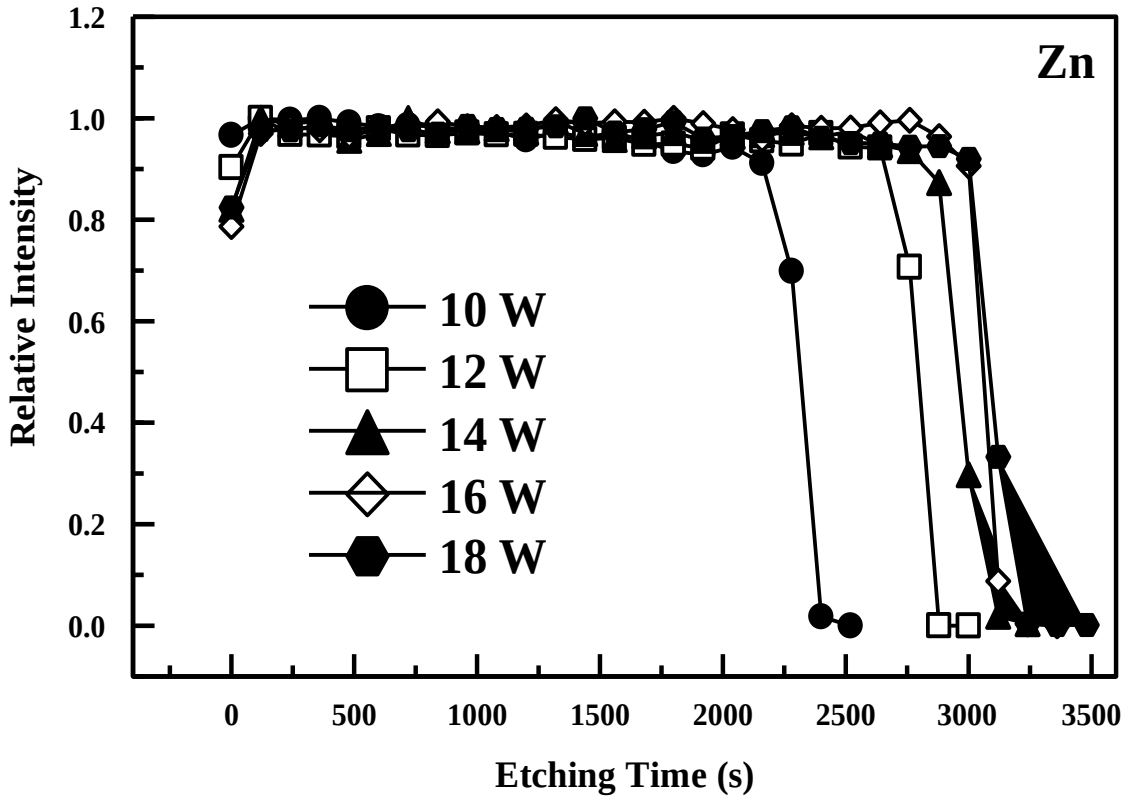

Figure 3.9. XPS depth profile of a co-sputtered film using 18-W DC power applied to the copper target, showing the relative intensity of Zn as a function of etching time.

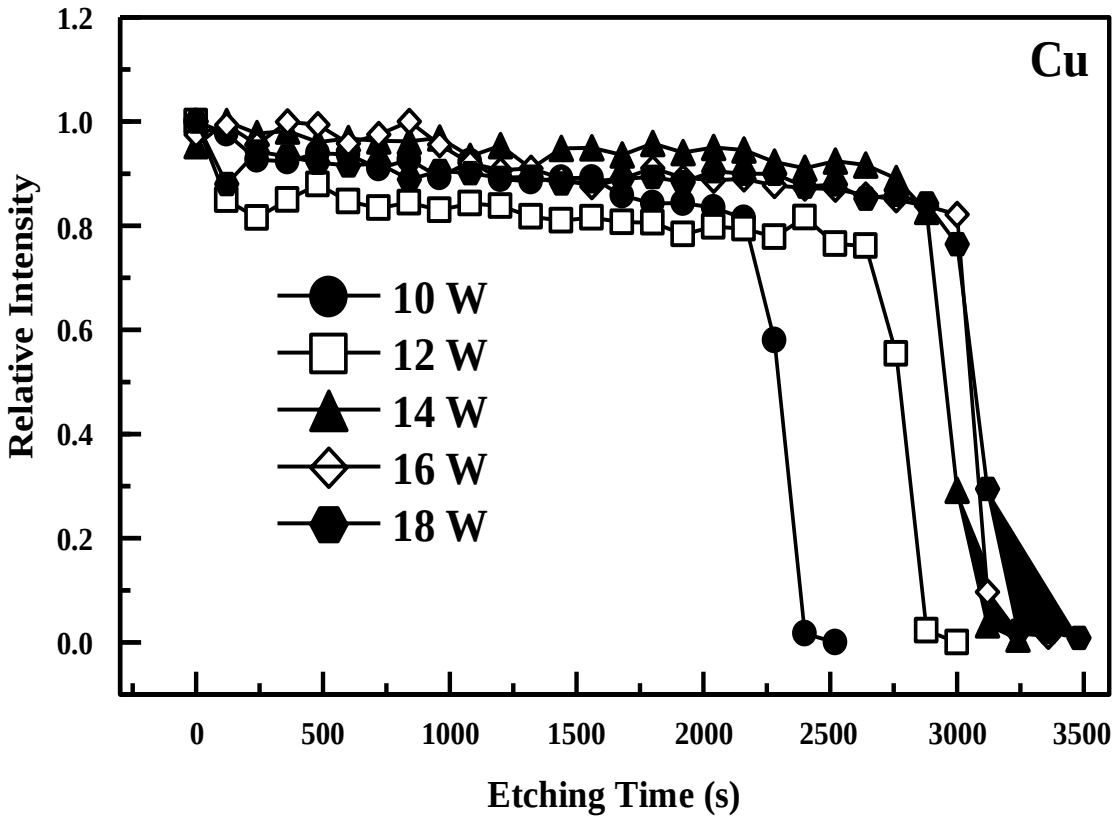

Figure 3.10. XPS depth profile of a co-sputtered film using 18-W DC power applied to the copper target, showing the relative intensity of Cu as a function of etching time.

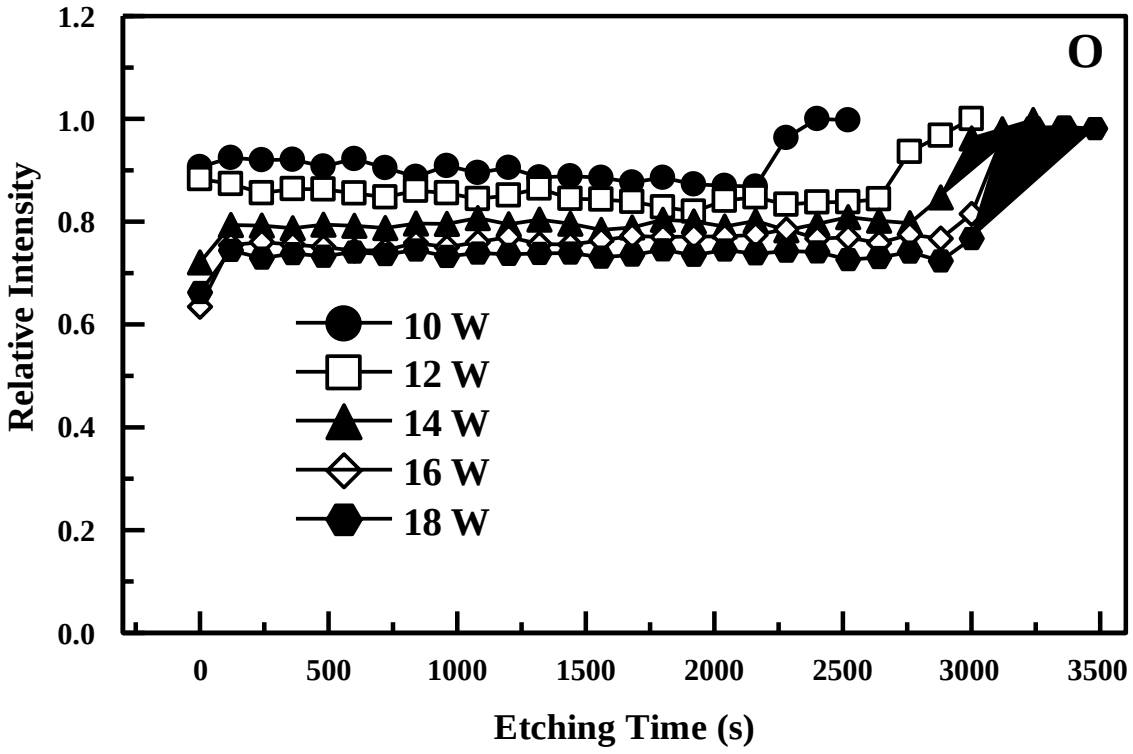

Figure 3.11. XPS depth profile of a co-sputtered film using 18-W DC power applied to the copper target, showing the relative intensity of O as a function of etching time.

CHAPTER 4

OPTICAL CHARACTERISTICS

Zinc oxide (ZnO) these times have emerged as potentially superior semiconductors for ultraviolet (UV) optoelectronics, including applications blue laser diodes [58] and photodetectors [59]. Nevertheless, several applications necessitate a significant absorption of visible light. These include photocatalysis [60], photovoltaics [61], the photoelectrochemical splitting of water [17], and photonic devices based on quantum well structures [62, 63]. The band gap of ZnO is rather large for an efficient absorption in the visible region, and therefore it is crucial to reduce and tune the band gap to enable the above-mentioned applications [17]. Table 4.1 is a compilation of the band gap of doped ZnO thin films deposited by various techniques. It clearly reflects the strong influence of the dopant and the deposition technique on the extent of band gap reduction. The band gap of zinc oxide thin films can be reduced through doping zinc oxide with copper. The band gaps of copper oxides are distinctively lower than that of zinc oxide. Optical applications require knowledge about the optical properties of the material. These include the absorption coefficient (α) and the band gap E_g. The optical properties of copper-doped zinc oxide thin films are sensitively dependent on the preparation conditions and the models used to extract the optical constants from measured quantities.

The transmittance and absorption spectra of the films are shown in figures 4.1 and 4.2, respectively. The un-doped ZnO thin films exhibited high transparency in the visible region. Copper doping resulted in a considerable reduction in transmittance, indicating

strong absorption in the visible range. The absorption edge shifted to higher wavelengths (red shift) as the copper concentration increased. The absorption coefficient (α) of the films were calculated using the equation:

$$\alpha = \left(\frac{1}{d}\right) ln \left(\frac{1}{T}\right) \quad (4.1)$$

where d is the thickness of the film and T is its transmittance. Figure 4.3 shows the variation of the absorption coefficient as a function of photon energy. The absorption coefficient is related to the band gap (E_g) through the relation:

$$\alpha E = A\,(E - Eg)^{\eta} \quad (4.2)$$

where A and η are constants, and E is the incident photon energy. Both zinc oxides and the copper oxides are direct band gap semiconductors [3, 64], and therefore η = 1/2. The band gap is obtained by plotting $(\alpha E)^2$ vs. E (Tauc plot), as shown in figure 4.4. Extrapolation of the linear portions of the curves to the energy axis gives the values of the band gaps. The band gap for pure ZnO was found to be 3.19 eV, which is in close agreement with previously reported values [30]. The band gap values for the copper-doped films were found to vary with the Cu concentrations (x) as listed in table 4.2. Thus, the band gap of ZnO was reduced by δ = 0.57 eV as a result of copper doping. The variation in the band gap with the Cu concentration can be fitted using a quadratic equation of the form [65]:

$$E_g(x) = (1 - x)\, E_g^{ZnO} + x\, E_g^{CuOx} - b\, x\, (1 - x) \quad (4.3)$$

where b is called the bowing coefficient, which describes the deviation from a linear relation between E_g and x. Our values for E_g were fitted using the above equation, as shown in figure 4.5, with a bowing coefficient of 0.060 eV, which indicates insignificant deviation

from linearity. The resulting value for E_g^{ZnO} was 3.16 eV, which is in close agreement to our experimental value of 3.19 eV. Extrapolation of the fit to x = 1 yields a value of 2.03 eV forE_g^{CuOx}, which is close to the value of 2.10 eV reported for Cu_2O thin films [64], suggesting that copper existed in the Cu^{+1} oxidation state, as found by XPS. Several previous studies [6, 17, 30, 31, 52] reported a reduction of the band gap of ZnO upon doping with copper, with values of δ that ranged from 0.05 eV [6] to 0.40 eV [31]. The decrease is expected since copper oxides have lower band gap values [30, 52]. Moreover, hybridization of the Cu 3d bands with O 2p bands leads to an exchange interaction that reduces the band gap of copper-doped ZnO [52].

Table 4.1. Band gap (E_g) tunability of ZnO thin films using elemental dopants

Dopant	Deposition Technique[(1)]	Dopant Concentration	E_g Range (eV)	Ref.
Ag	SP	5-25 mol%	2.98-3.12	[66]
Bi	Sol-gel	0.3-10 mol%	3.08-3.25	[67]
Cd	Sol-gel	5-30 at%	3.16-3.27	[68]
	Sp	1-25 at%	2.94-3.25	[69]
	PLD	2-8 %	2.90-3.28	[62]
Co	Sol-gel	1-8 %	2.85-3.22	[70]
	SP	5-20 at%	2.76-2.92	[71]
	SP	0.2-1 wt%	2.79-3.22	[72]
Cu	RFS	3-10 at%	3.05-3.25	[17]
	SP	2-20 at%	2.72-3.12	[31]
F	SP	0.5-5 at%	3.09-3.30	[73]
Fe	RFS	5.2-21.2 %	2.8-3.3	[74]
	Spin coating	6-10 at%	3.04-3.23	[75]
Hf	Sol-gel	1-6 mol%	3.17-3.26	[76]

In	Sol-gel	0.69-2.34 at%	3.08-3.19	[77]
	SP	2-8 at%	3.09-3.20	[78]
Mn	MBE	3-33 %	2.7-3.3	[79]
N	PLD	0.2-0.7 at%	3.1-3.3	[80]
Na	Sol-gel	2-10 %	3.12-3.26	[81]
Ni	RFS	3.5-6 at%	2.80-3.34	[82]
Sn	SP	1-2 at%	2.87-3.13	[83]

(1)MBE: molecular beam epitaxy; PLD: pulsed laser deposition; RFS: radio-frequency sputtering; SP: spray pyrolysis

Table 4.2. Band gap (E_g) of the films as function of the DC power applied to the Cu target

Property	DC Power (W)					
	0	10	12	14	16	18
E_g (eV)	3.19	2.79	2.76	2.72	2.69	2.62

E_g = band gap

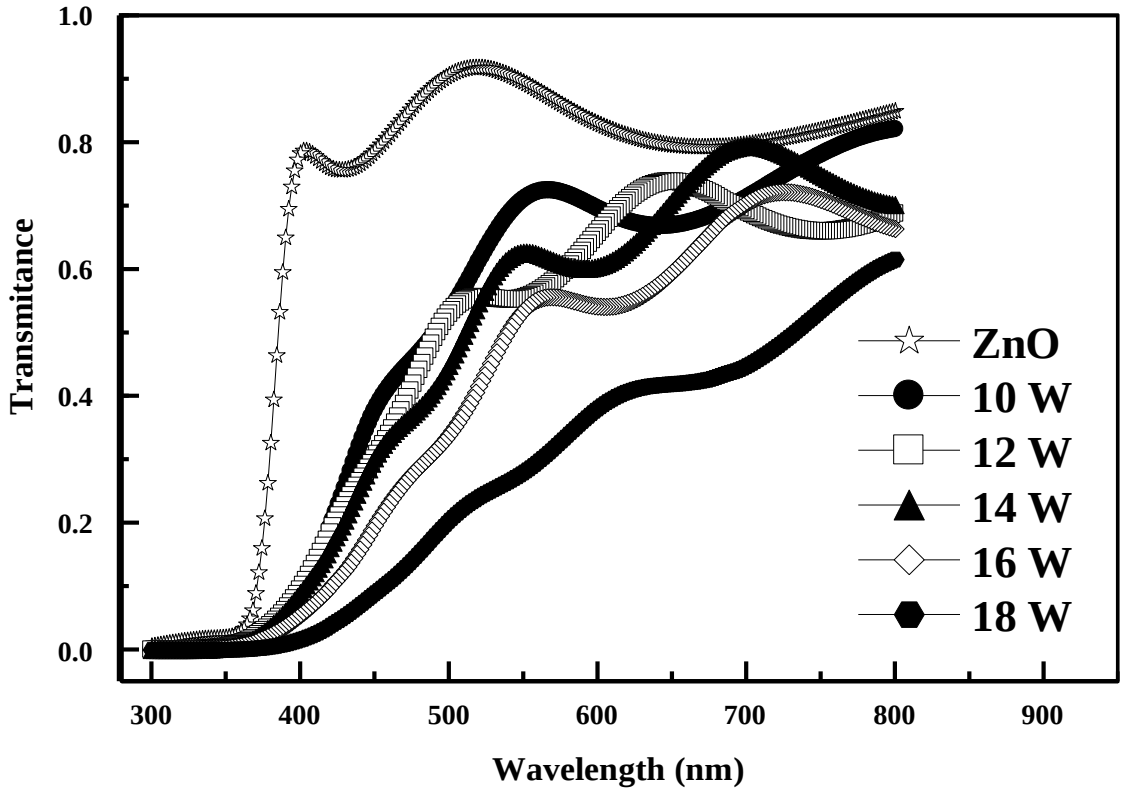

Figure 4.1. Measured normal incidence transmittance spectra of the films.

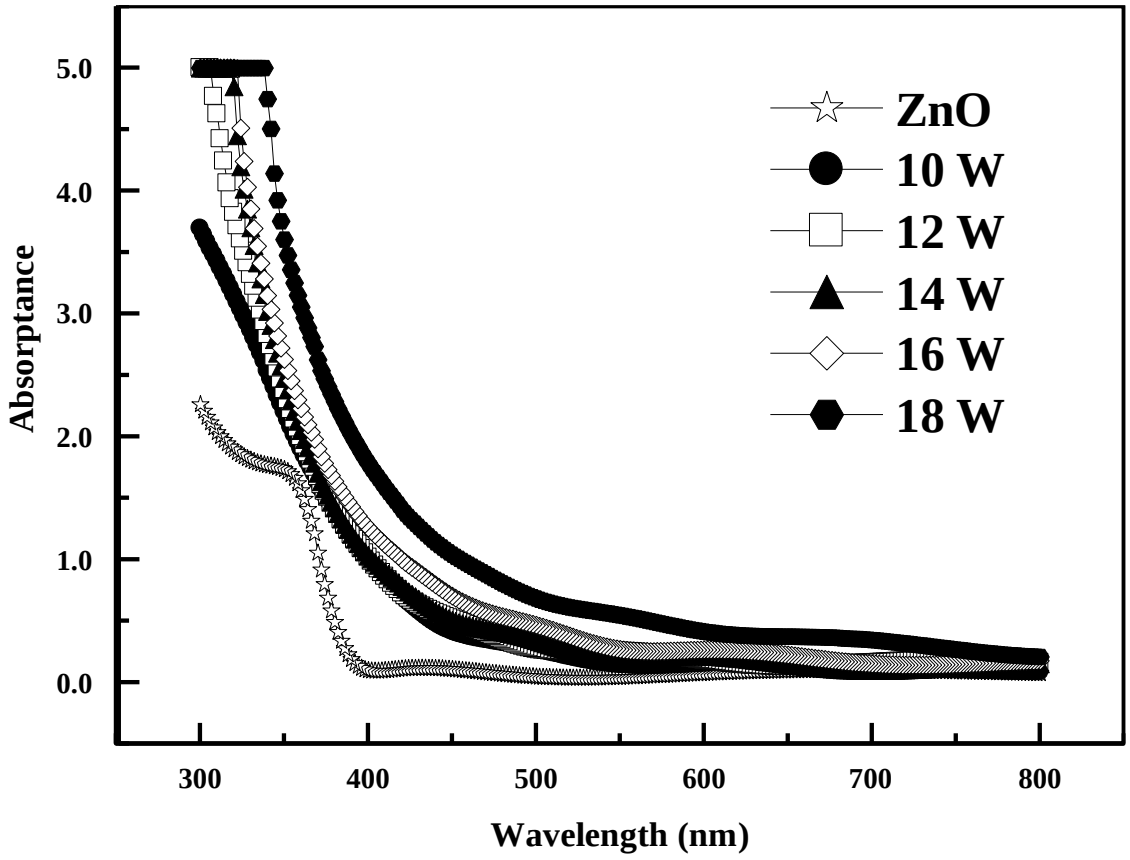

Figure 4.2. Measured normal incidence absorption spectra of the films.

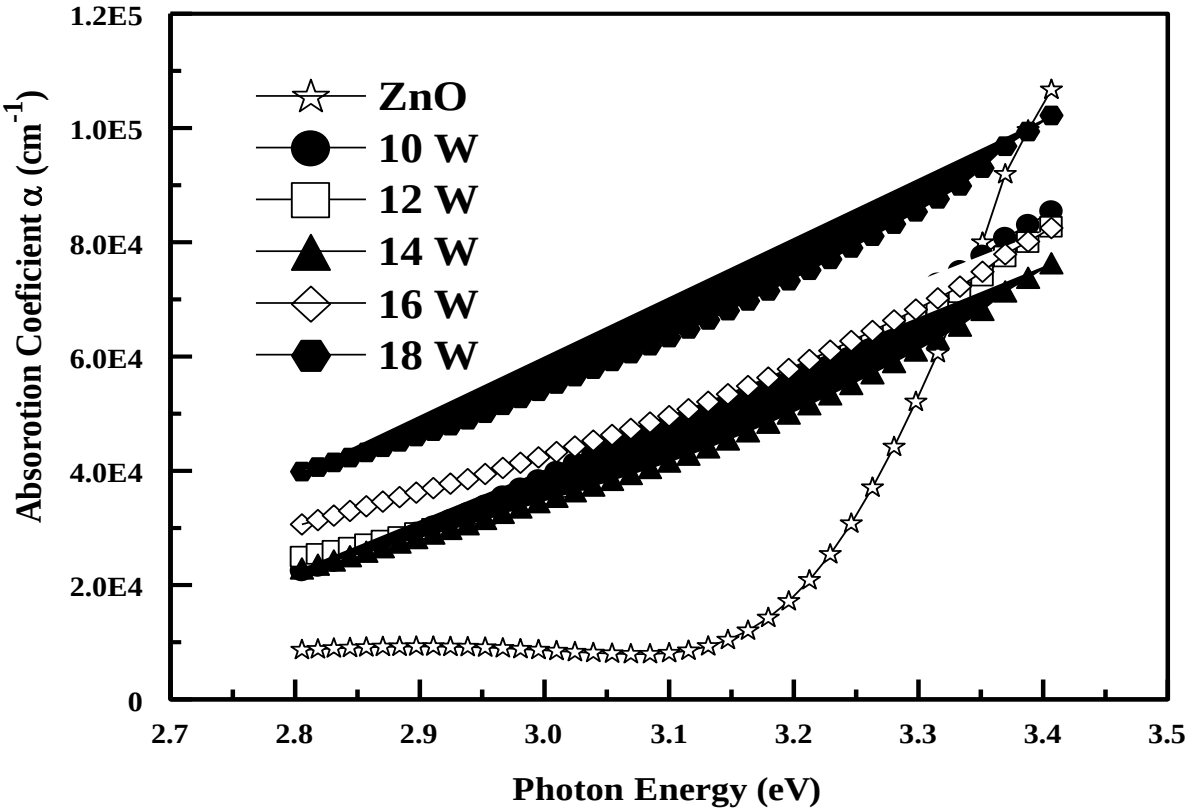

Figure 4.3. Dependence of the absorption coefficient of the films on photon energy.

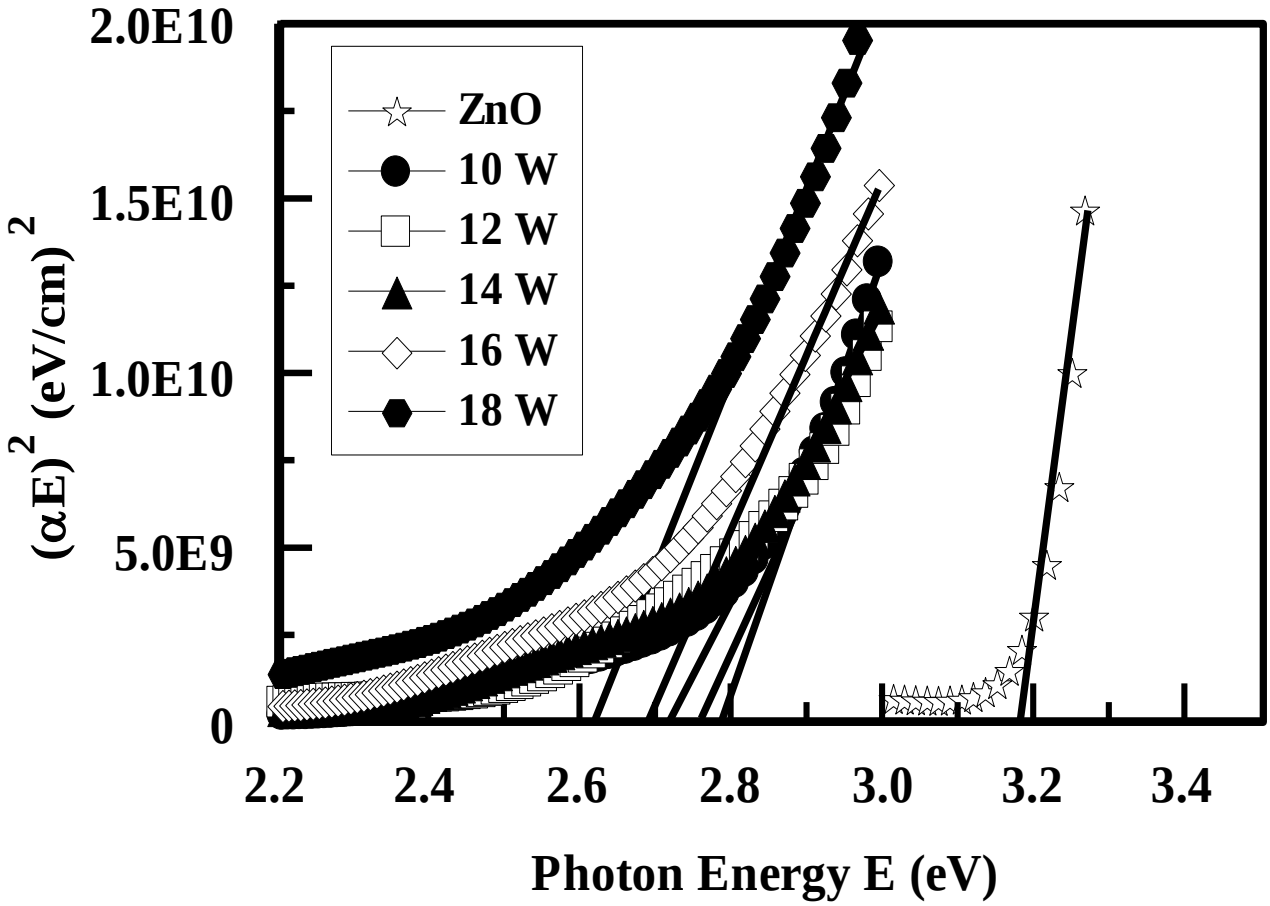

Figure 4.4. Tauc plots showing the dependence of the band gap of the films on photon energy.

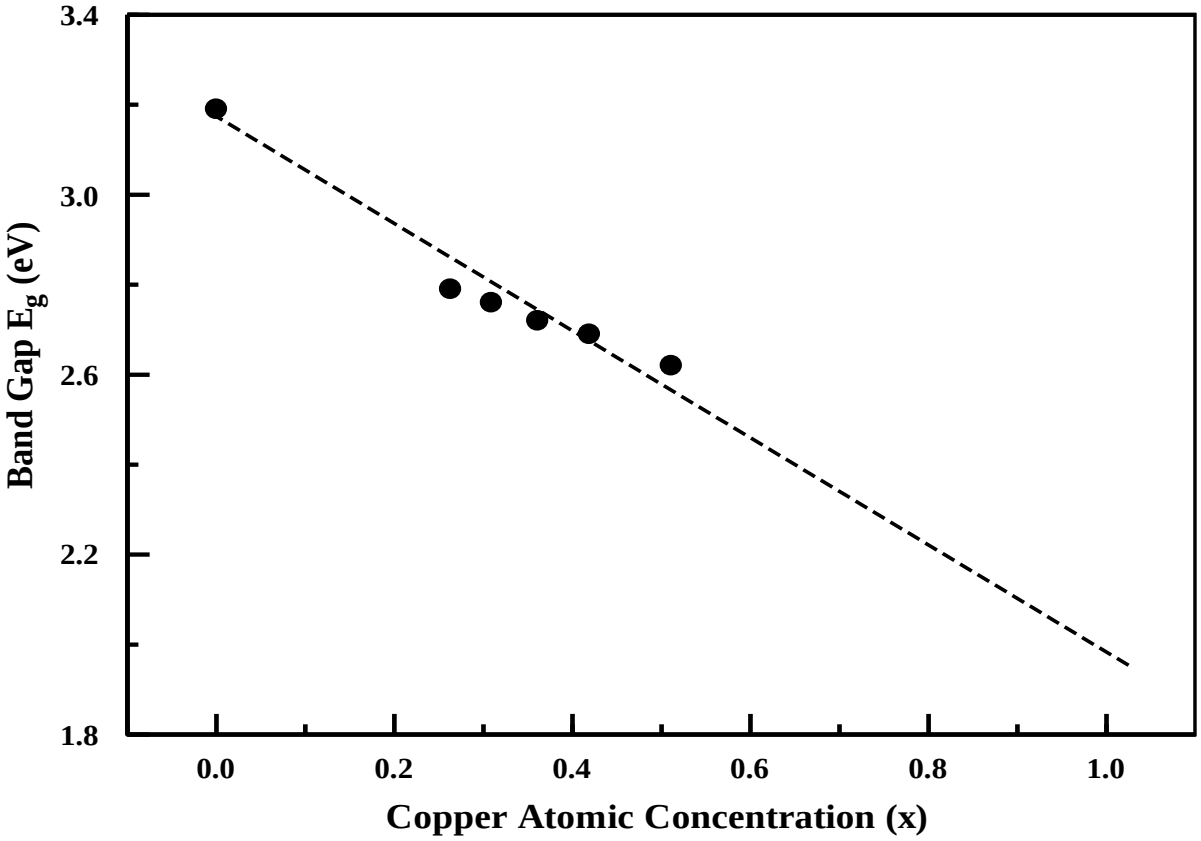

Figure 4.5. Dependence of the band gap of the films on the atomic concentration of copper

CHAPTER 5

ANNEALING IN OXYGEN

Deposition of copper-doped zinc oxide thin films was carried out by magnetron co-sputtering technique. The deposition was done at room temperature. After deposition, the as-deposited thin films under a DC power of 18 W applied to the Cu target were annealed in oxygen in a horizontal tube furnace at a temperature of 400 ˚C. The furnace was evacuated to a base pressure 5×10^{-4} mbar. Then oxygen was admitted at a flow rate of 50 sccm. The annealing treatment was carried out for 4 hours. Upon completion of annealing, the specimens were naturally cooled down to room temperature while they were still in the furnace. The effect of the annealing on the structural, chemical, optical, and electrical properties of the copper-doped zinc oxide thin films were executed through X-ray diffraction (XRD), atomic force microscopy (AFM), spectrophotometry, X-ray photoelectron spectroscopy (XPS) and resistivity measurements.

5.1 STRUCTURAL PROPERTIES

X-ray diffraction patterns of annealed thin films were investigated in order to determine the structure characteristics. XRD revealed that the as-deposited and annealed films were amorphous.

5.2 MORPHOLOGICAL PROPERTIES

The surface morphology studies of the as-deposited and annealed thin films were analyzed with the help of atomic force microscopy (AFM). Figures 5.1 and 5.2 show three and two dimensional AFM images of the films, respectively. The surface roughness and grain size values are listed in table 5.1. The morphology of the as-deposited thin films was characterized by regular grains with a grain size value of 26.9 nm. The surface roughness and grain size of the films increased with annealing. The grain size increased because of the coalescence of the smaller grains due to thermal energy. Consequently, the surface roughness increased.

5.3 OPTICAL PROPERTIES

To reveal the annealing effects on the optical properties, we measured the transmission and absorption. Figures 5.3 and 5.4 show the transmittance and absorption spectra for the as-grown and annealed films, respectively. The transmittance spectra of the films changed significantly with annealing. Annealing resulted in a considerable reduction in transmittance which may due to enhanced absorption in the visible region. The variation of the absorption coefficient as a function of photon energy (E) is shown in figure 5.5. The Tauc plots of $(\alpha E)^2$ versus (E) for the as-grown and annealed thin films are shown in figure 5.6. The band gap of the as-deposited thin films was found to be 2.62 eV. After annealing, the band gap reduced to 2.25 eV. These values indicate that annealing decreased the band gap of the films by oxidizing copper, where copper oxides have band gaps that are less than that of zinc oxide.

5.4 ELECTRICAL PROPERTIES

The resistivity of the films was measured using the two-probe technique. This method is especially suited for highly-resistive films. In this technique, two gold contacts were thermally evaporated on the films. The geometry of the contacts is shown in figure 5.7-a. Then, a bias voltage (*V*) was applied across these two contacts, and the current (*I*) was measured. The current-measurement circuit is shown in figure 5.7-b. The external circuit was connected to the gold contacts using silver past. The bias voltage application and the current measurement were performed automatically using a Keithley 238 measure unit, which was interfaced to a computer using LabVIEW. The bias voltage was swept from -5V to +5V. The *I-V* curves of the films are shown in figure 5.8. The inverse of its slope is the resistance (*R*) of the film. The resistivity of the film was calculated using Ohm's law:

$$R = \rho \frac{L}{A} \qquad (5.1)$$

In our case, the area $A = w \times d$, where w is the length of the gold contact, and d is the thickness of the film (figure 5.7a). From which, the resistivity can be written as:

$$\rho = \frac{Rwd}{L} \qquad (5.2)$$

For all measurements, w = 2.2 cm and L = 0.17 cm. The resistivity measured in this manner for all films is listed in table 5.1. The value of the resistivity changed significantly for the annealed film. This decrement of resistivity may be correlated with the oxidation of copper.

5.5 CHEMICAL ANALYSIS

The O1s spectrum of the annealed films has a complicated structure because of the pressure of several types of oxygen species. The O1s can be decomposed into three components as shown in figure 5.9. The first component (A) at a binding energy of 529.8 eV corresponds to oxygen bonded to zinc and copper. The second component (B) at a binding energy of 531.2 eV corresponds to oxygen atoms in oxygen deficient regions (i.e. oxygen vacancies). This component is responsible for the enhancement of electrical conductivity since these oxygen vacancies behaves as electron donors. The third component (C) in the O1s spectrum is at the high binding energy side at a binding energy 531.6 eV and corresponds to loosely bond surface oxygen species (such as CO^{-}_{3}, OH^{-}, adsorbed H_2O, and adsorbed O_2).

Table 5.1. Physical properties of as-deposited and annealed thin films.

Property	DC Power (W)				
	d (nm)	R_{rms} (nm)	GS (nm)	ρ (Ω.cm)	E_g (eV)
As-deposited	711	1.5	26.9	4.6×10^{5}	2.62
Annealed	692	11.6	34.6	4.5×10^{3}	2.25

d = Film thickness, R_{rms} = root-mean-square surface roughness, GS = Grain Size, ρ = Resistivity, E_g = Band Gap

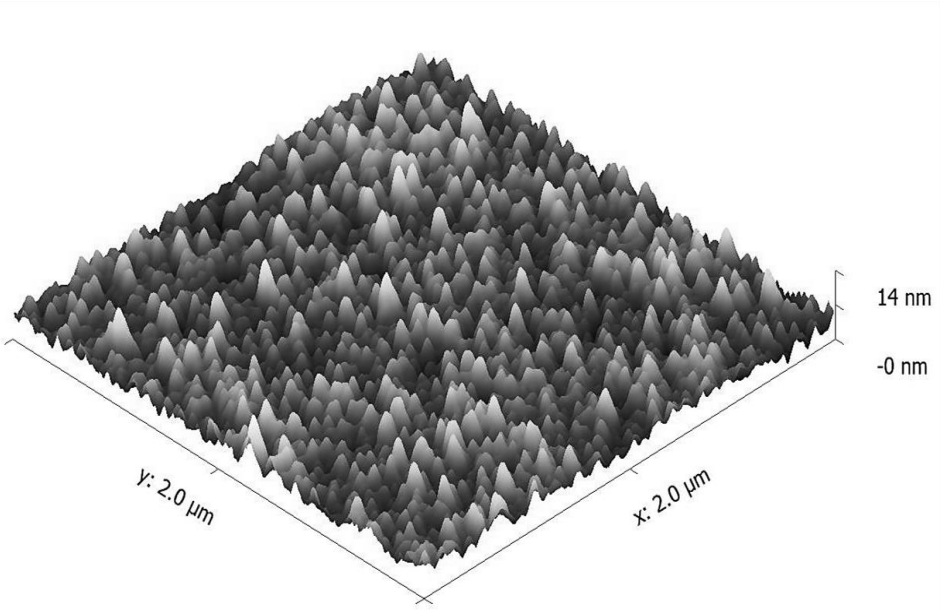

as-deposited

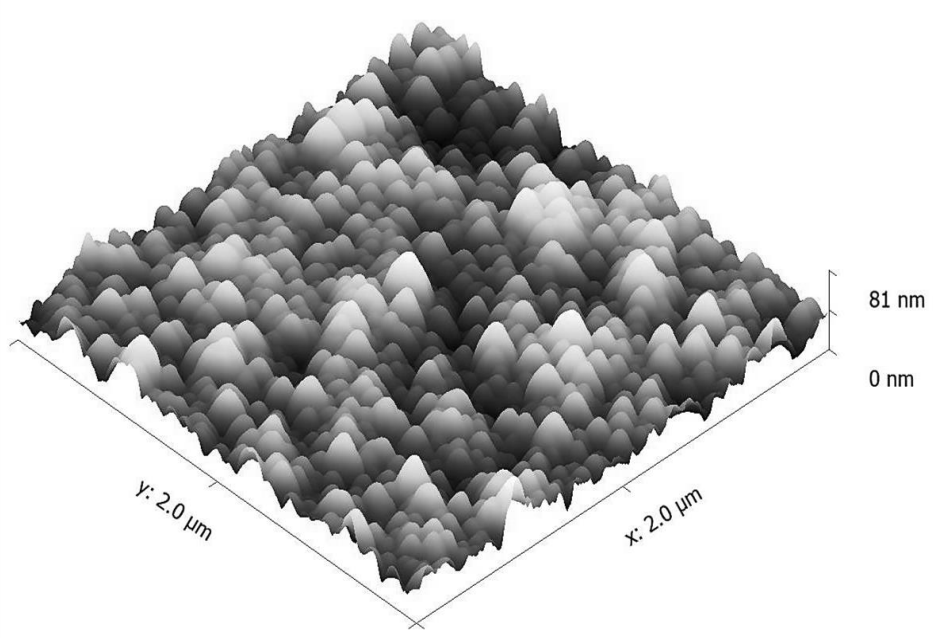

annealed in oxygen

Figure 5.1. Three-dimensional AFM micrographs of as-deposited and annealed thin films. The DC power applied to the Cu target was 18 W

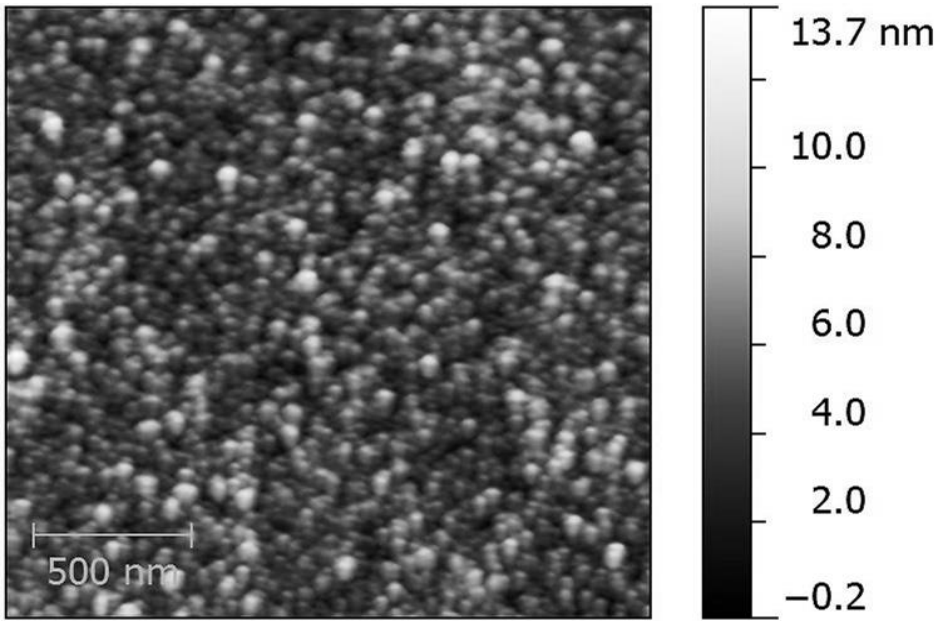

as-deposited

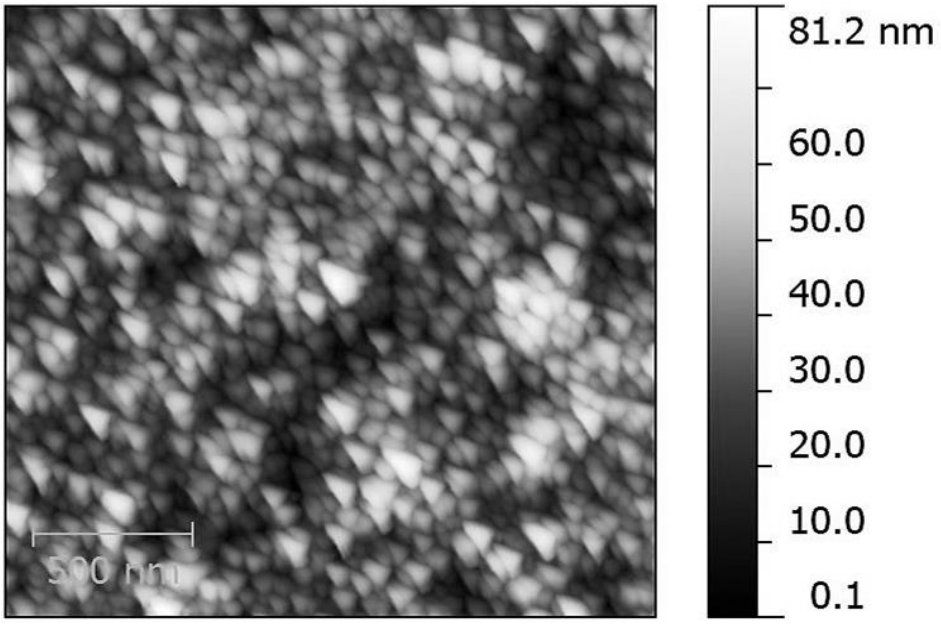

annealed in oxygen

Figure 5.2. Two-dimensional AFM micrographs of as-deposited and annealed thin films. The DC power applied to the Cu target was 18 W

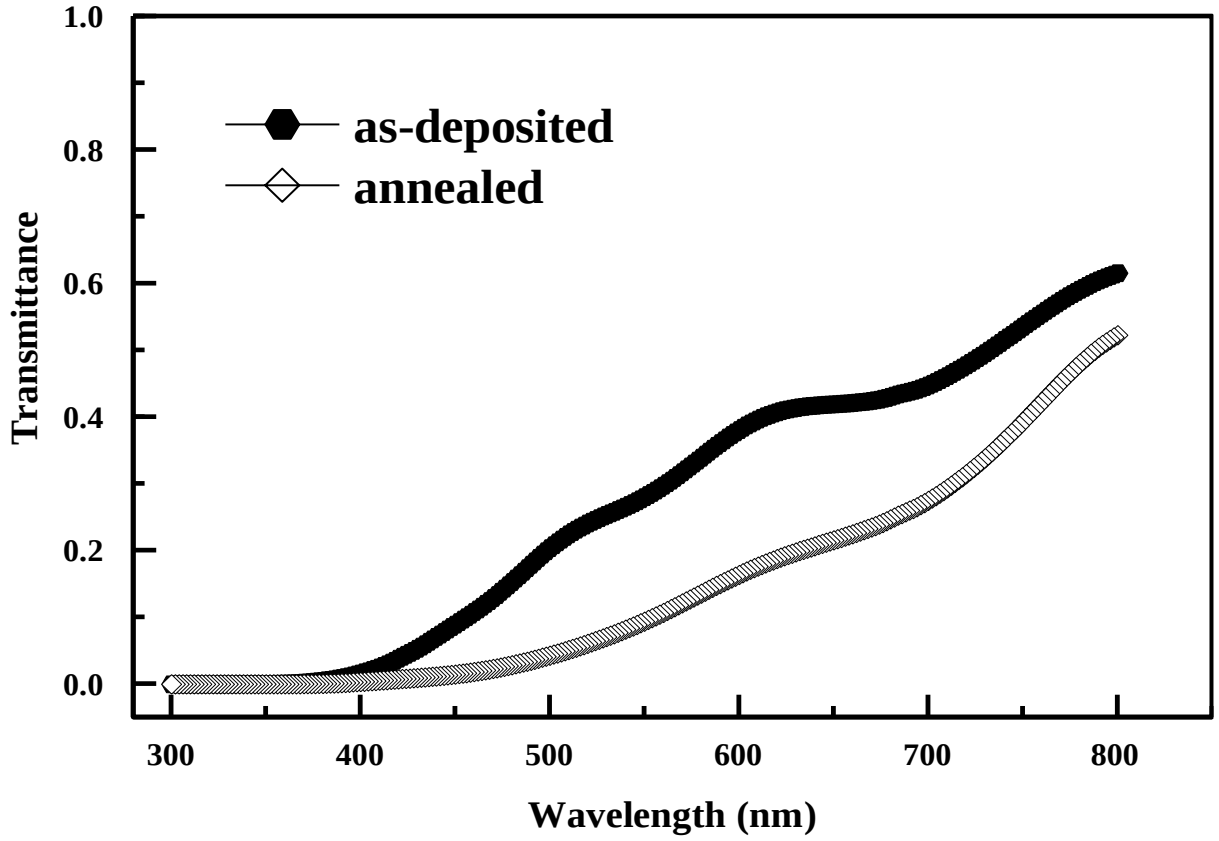

Figure 5.3. Measured normal incidence transmittance spectra of the films deposited under an 18 W DC power and annealed in oxygen

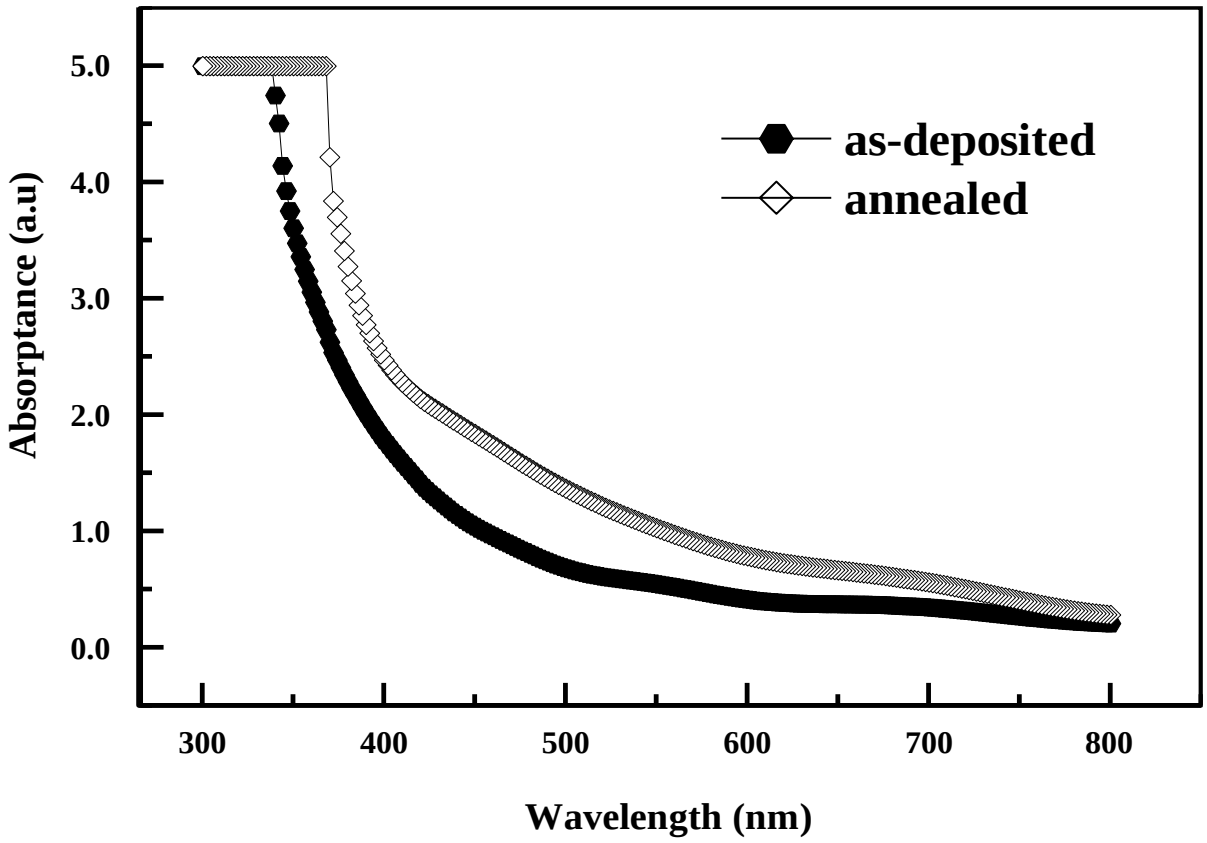

Figure 5.4. Measured normal incidence absorption spectra of the films deposited under an 18 W DC power and annealed in oxygen.

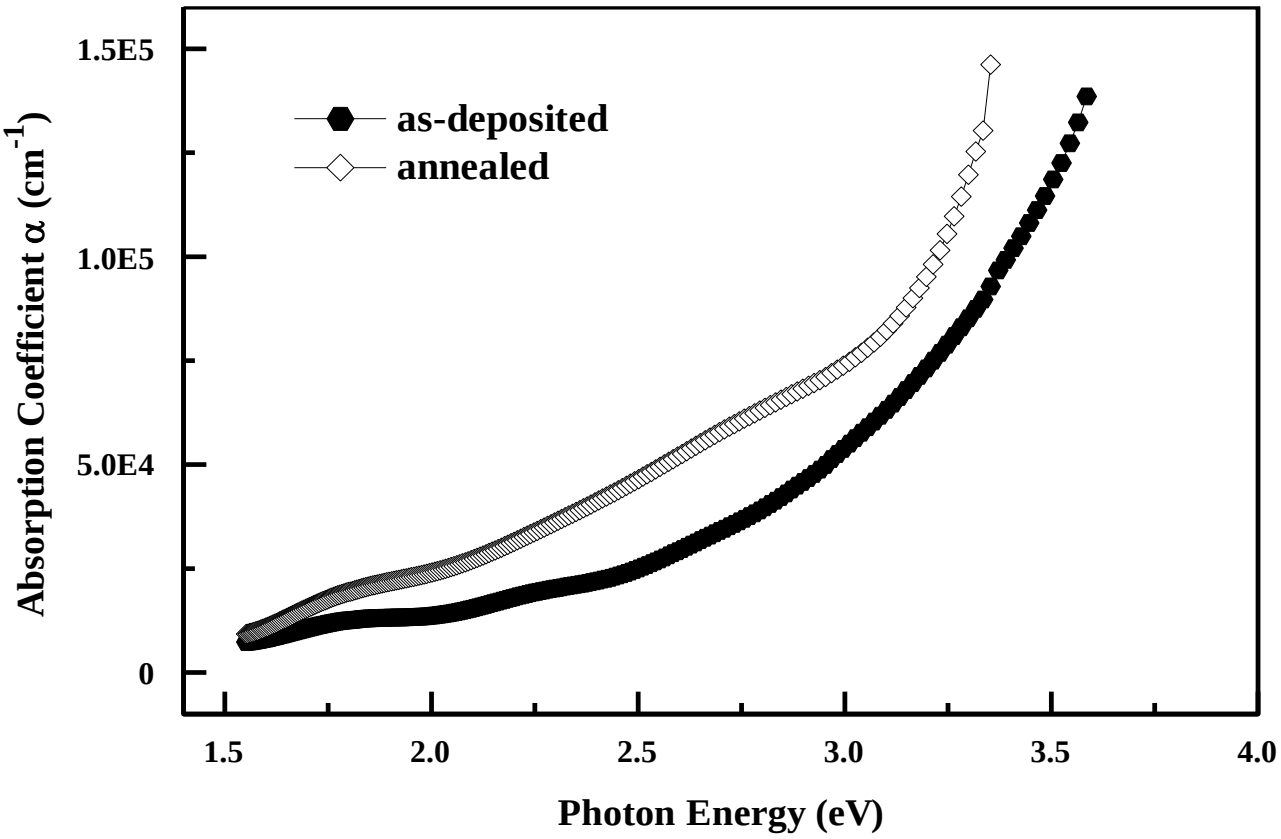

Figure 5.5. Dependence of the absorption coefficient of the films deposited under an 18 W DC power and annealed in oxygen on photon energy**.**

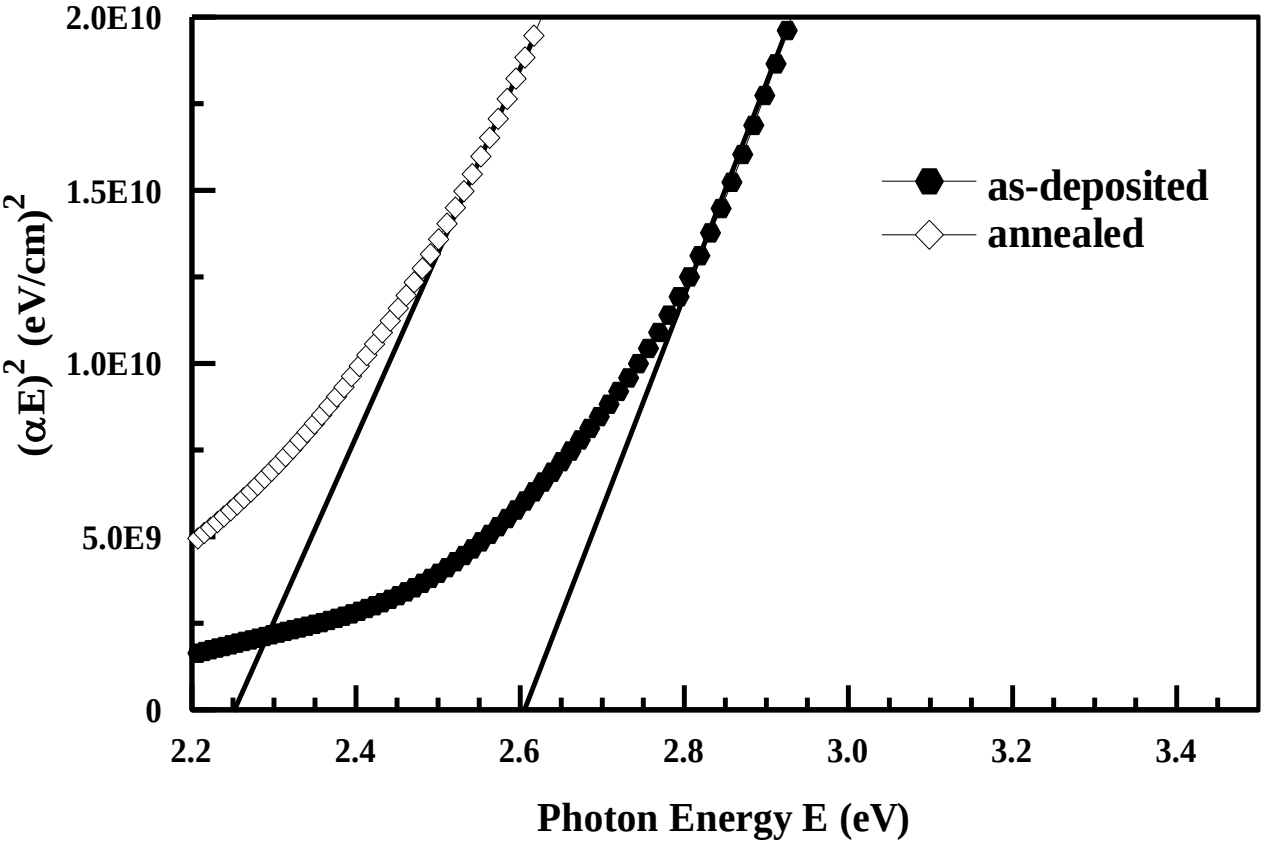

Figure 5.6. Tauc plots showing the dependence of the band gap of the films deposited under an 18 W DC power and annealed in oxygen on photon energy.

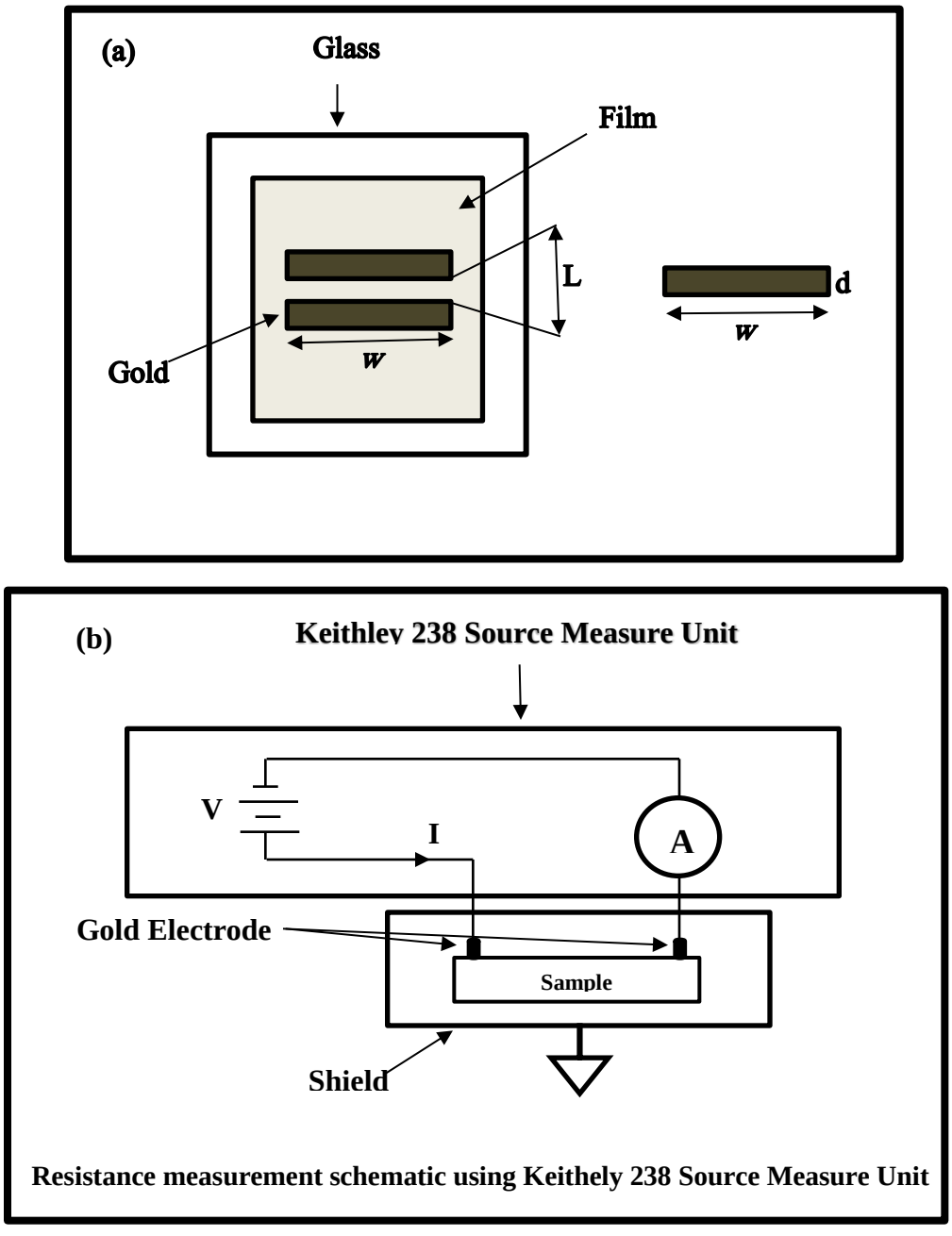

Figure 5.7. Details of the electric measurement system. (a) Geometry of the gold contacts. (b) Measurement circuit.

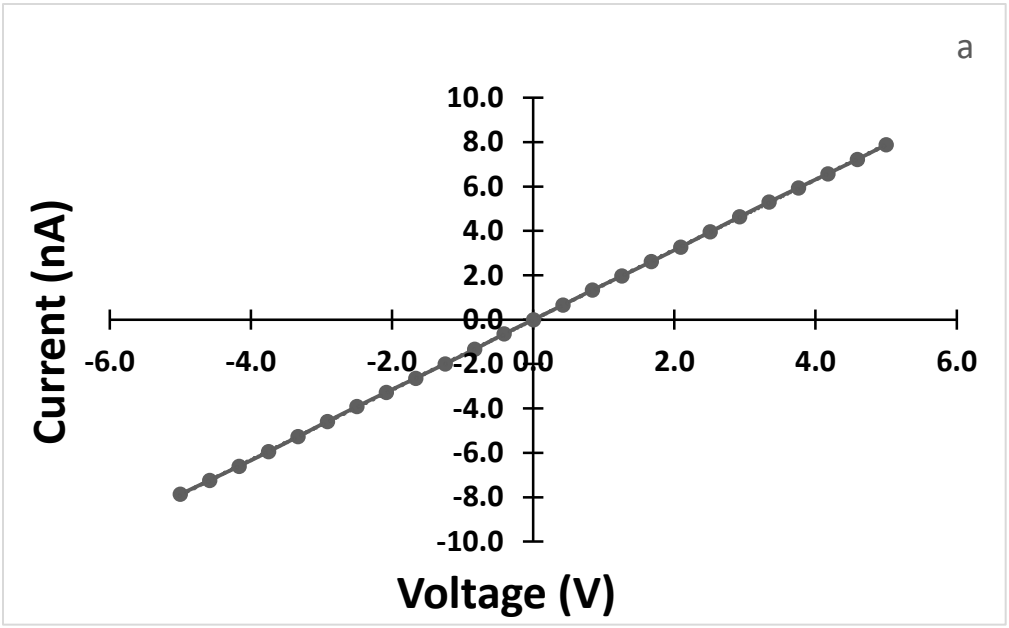

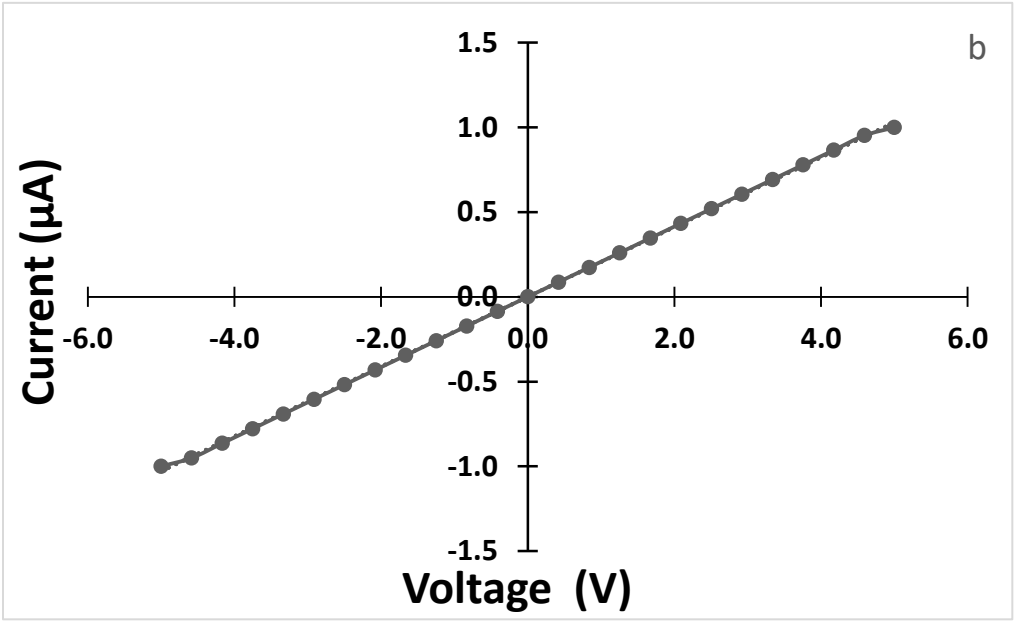

Figure 5.8. Current-Voltage curves of as-deposited sample (a) and annealed sample (b).

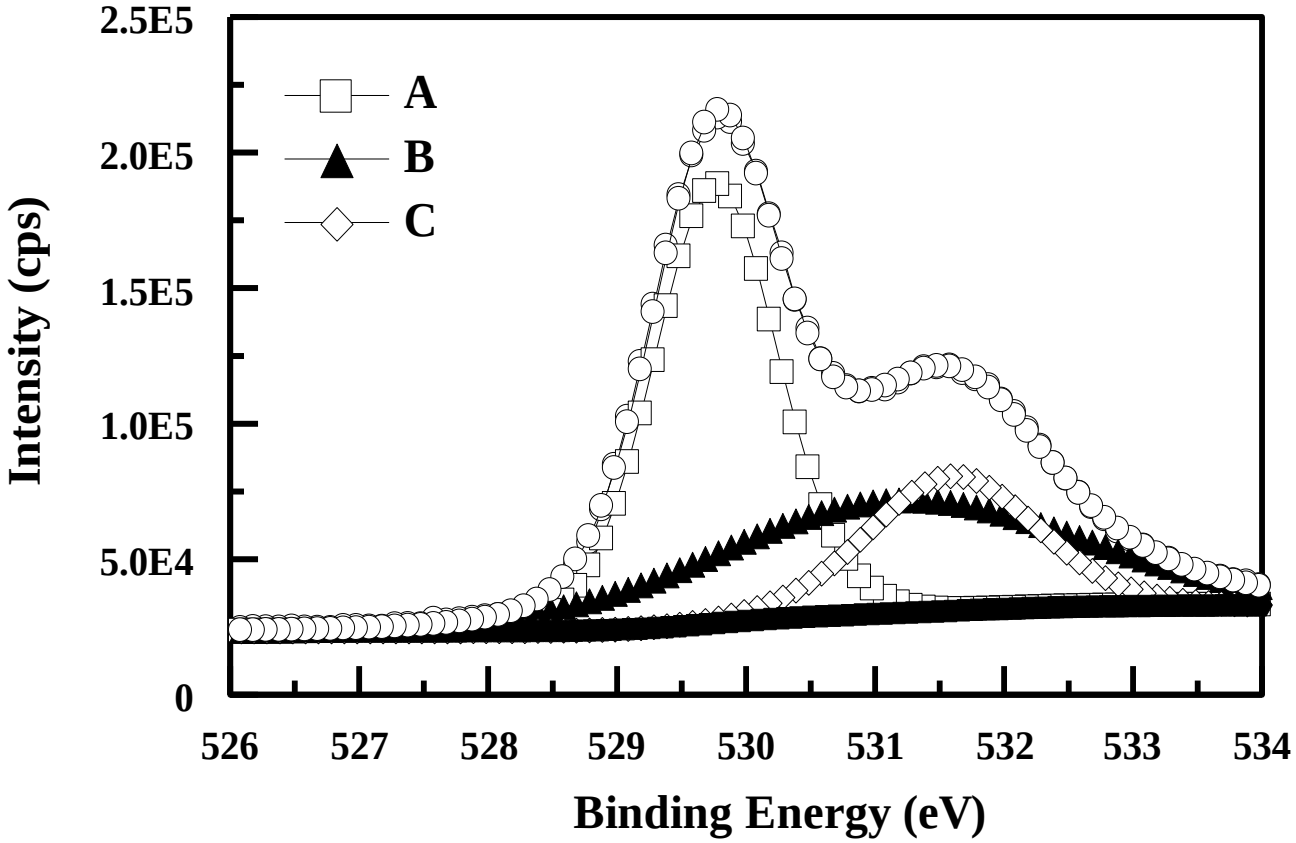

Figure 5.9 O1s XPS spectrum of an annealed thin film. The spectrum was resolved into its three components. The experimental spectrum is denoted by the open circles.

CHAPTER 6

CONCLUSIONS AND FUTURE SUGGESTIONS

6.1 CONCLUSIONS

Copper-doped zinc oxide thin films were deposited by co-sputtering, where a fixed 100 W RF power was applied to a ZnO target and a variable DC power (10-18 W) was applied to a copper target. The annealing of the films deposited under 18 W was investigated at 400 $^{\circ}$C in an oxygen environment. From the work, the following conclusions can be made.

- The thickness of the films was increased from 302 nm to 711 nm as the DC sputtering power increased.
- The pure zinc oxide thin films and those deposited under a DC power of 10 W showed growth oriented along the (002) direction of the hexagonal wurtzite structure of ZnO, whereas those deposited under higher DC powers were amorphous.
- The morphology of the surfaces of the films exhibited a columnar microstructure.
- The surface roughness of the deposited films was decreased with an increase in copper concentration, whereas the grain size of the films fluctuated.
- Chemical analysis indicated that zinc exists only as the oxidized state, and copper also existed in an oxidized state, specifically the Cu_2O phase, and that the elements were homogeneously distributed through the thickness of the film.

- The atomic concentration of copper was increased as the DC sputtering power increased, resulting in ZnO thin films that were heavily doped with 26.3-51.1 at% of copper.
- The pure ZnO films were highly transparent in the visible range, with a band gap of 3.19 eV. Transparency was significantly reduced upon copper doping due to strong absorption.
- The absorption edge shifted to higher wavelengths as the copper concentration increased.
- The band gap of the doped films showed a continuous decrease as the copper concentration increased, reaching a value of 2.62 eV for 51.1 at% of copper, which amounts to a considerable red shift of the band gap of ZnO by a value of 0.57 eV.
- Annealing did not influence the crystallinity of the films deposited under a DC power of 18 W, which were still amorphous.
- In case of the annealed films, surface roughness and grain size were increased by annealing.
- The band gap and resistivity of the deposited films under a DC power of 18 W were decreased by annealing them in an oxygen environment.

6.2 SUGGESTIONS

- Investigate the effects of substrate temperature, RF power, and argon flow rate.
- Investigate the effects of the annealing in vacuum and hydrogen.
- Investigate the magnetic characteristics of copper-doped zinc oxide thin films prepared by magnetron co-sputtering.
- Investigate the uses of copper-doped zinc oxide thin films in applications such as:
    i. Spintronic applications.
    ii. Gas sensing.
    iii. Photocatalysis.
    iv. Photovoltaics.

References

[1] M. Garcia, J. Rodriguez, *Metal oxide nanoparticles*, Brookhaven National Laboratory. (2007) 79479.

[2] C. Klingshirn, B. Meyer, A. Waag, A. Hoffmann, J. Geurts, *Zinc oxide from fundamental properties towards novel applications*, Spring Series in Materials Science 120, Spring-Verlag, Berlin (2010).

[3] C. Jagadish, S. Pearton, *Zinc oxide bulk, thin films and nanostructures processing, properties and applications*, First Edition, Elsevier Science (2006).

[4] M. Caglar, F. Yakuphanoglu, *Structural and optical properties of copper doped ZnO films derived by sol–gel*, Applied Surface Science. 258 (2012) 3039–3044.

[5] H. Al-Khanbashi, W. Shirbeeny, A. Al-Ghamdi, L. Bronstein, W. Mahmoud, *Development of highly conductive and transparent copper doped zinc oxide thin films via 2-methoxyethanol modified sol–gel dip-coating technique*, Ceramics International. 40 (2014) 1927–1932.

[6] Y.Chen, X. Xu, G. Zhang, H. Xue, S. Ma, *Comparative study of the microstructures and optical properties of Cu- and Ag-doped ZnO thin films*, Physica B. 404 (2009) 3645–3649.

[7] https://en.wikipedia.org/wiki/Zinc_oxide, (n.d.).

[8] M. Ferhat, A. Zaoui, R. Ahuja, *Magnetism and band gap narrowing in Cu-doped ZnO*, Applied Physics Letters. 94 (2009) 142502.

[9] H. Liu, P. Zhou, L. Zhang, Z. Liang, H. Zhao, *Effects of oxygen partial pressure on the structura land optical properties of undopedand Cu-doped ZnO thin films prepared by magnetron co-sputtering*, Materials Letters.164 (2016) 509–512.

[10] H. Pozos, E. Arredondo, A. Álvarez, R. Biswal, Y. Kudriavtsev, J. Pérez, Y. Moreno, M. Amador, *Cu-doped ZnO thin films deposited by a sol-gel process using two copper precursors: gas-sensing performance in a propane atmosphere*, Materials. 9 (2016) 87.

[11] L. Engström, *The copper book for architecture*, Second edition, Aurubis-Copper Book for Architecture. (2013) 17-28.

[12] M. Kutz, *Mechanical Engineers' Handbook: Materials and Mechanical Design*, John Wiley & Sons, Inc.1 (2006) 117-127.

[13] H. Jing, Z. Yu, L. Li, *Antibacterial properties and corrosion resistance of Cu and Ag/Cu porous materials*, Wiley Inter Science. (2007) 31688.

[14] W. Lanford, P. Ding, W. Wang, S. Hymes, S. Murarka, *Alloying of copper for use in microelectronic metallization*, Materials Chemistry and Physics. 41 (1995) 192-198.

[15] R. Ritasalo, *Properties of pulsed electric current sintered copper and copper composites*, School of Chemical Technology. 53 (2014) 11-13.

[16] M. Zaman, *Synthesis, characterization, and device applications of viral-templated copper sulfide and copper oxide semiconductor nanomaterials*, eScholarship. (2014) 8-9.

[17] K. Ahn, T. Deutsch, Y. Yan, C. Jiang, Craig L. Perkins, J. Turner, M. Al-Jassim, *Synthesis of band-gap-reduced p-type ZnO films by Cu incorporation*, Journal of Applied Physics. 102 (2007) 023517.

[18] P. Zhou, H. Liu, L. Zhang, X. Sou, Z. Liang, Y. Liu, Y. Li, Z. Jiang, Z. Wang, *Study of substrate temperature and copper doping effects on structural, electrical and optical properties of Cu-doped and undoped ZnO thin films*, Journal of Materials Science: Materials in Electronics. 27 (2016) 7822-7828.

[19] Y. Liu, H. Liu, Y. Yu, Q. Wang, Y. Li, Z. Wang, *Structural and optical properties of ZnO thin films with heavy Cu-doping prepared by magnetron co-sputtering*, Materials Letters. 143 (2015) 319–321.

[20] G. Kim, D. Kim, B. Ahn, S. Lee, H. Kim, *Investigation on doping behavior of copper in ZnO thin film*, Microelectronics Journal. 40 (2009) 272–275.

[21] X. Cai, H. Liang, X. Xia, R. Shen, Y. Liu, Y. Luo, G. Du, *Influence of Cu dopant on the structure and optical properties of ZnO thin films prepared by MOCVD*, Journal of Materials Science: Materials in Electronics. 26 (2015) 1591–1596.

[22] A. Sreedhar, H. Jung, J. Kwon, J. Yi, J. Gwag, *Effect of ion beam assistance on Cu-doped ZnO thin films deposited by simultaneous RF and DC magnetron sputtering*, Ceramics International. 42 (2016) 3064–3071.

[23] P. Rai, S. Tripathy, N. Park, I. Lee, Y. Yu, *CTAB-assisted hydrothermal synthesis of single crystalline copper-doped ZnO nanorods and investigation of their photoluminescence properties*, Journal of Materials Science: Materials in Electronics. 21 (2010) 1036-1041.

[24] N. Kouklin, *Cu-doped ZnO nanowires for efficient and multispectral photodetection applications,* Advanced Materials. 20 (2008) 2190-2194.

[25] Q. Ma, D. Buchholz, R. Chang, *Local structures of copper-doped ZnO films,* Physical Review B. 78 (2008) 214429.

[26] N. Kamarulzaman, M. Kasim, N. Chayed, *Elucidation of the highest valence band and lowest conduction band shifts using XPS for ZnO and* $Zn_{0.99}Cu_{0.01}O$ *band gap changes*, Results in Physics. 6 (2016) 217–230.

[27] A. Kostruba, B. Kulyk, B. Turko, *Ellipsometric studies of optical properties of copper doped zinc oxide films on glass substrates*, Journal of Alloys and Compounds. 518 (2012) 96–100.

[28] C. Sudakar, J. Thakur, G. Lawes, R. Naik, V. Naik, *Ferromagnetism induced by planar nanoscale CuO inclusions in Cu-doped ZnO thin films*, Physical Review B. 75 (2007) 054423.

[29] T. Saidani, M. Zaabat, M. Aida, B. Boudine, *Effect of copper doping on the photocatalytic activity of ZnO thin films prepared by sol-gel method,* Superlattices and Microstructures. 88 (2015) 315-322.

[30] N. Tarwal, K. Gurav, S. Mujawar, S. Sadale, K. Nam, W. Bae, A. Moholkar, J. Kim, P. Patil, J. Jang, *Photoluminescence and photoelectrochemical properties of the spray deposited copper-doped zinc oxide thin films,* Ceramics International. 40 (2014) 7669–7677.

[31] G. Mani, J. Rayappan, *Influence of copper doping on structural, optical and sensing properties of spray deposited zinc oxide thin films*, Journal of Alloys and Compounds. 582 (2014) 414–419.

[32] A. Mhamdi, R. Mimouni, A. Amlouk, M. Amlouk, S. Belgacem, *Study of copper doping effects on structural, optical and electrical properties of sprayed ZnO thin films*, Journal of Alloys and Compounds. 610 (2014) 250–257.

[33] R. Malik, R. Khanna, G. Sharma, S. Pavunny, R. Katiyar, *Hydrogen sensing properties of copper-doped zinc oxide thin films*, IEEE Sensors Journal. 15 (2015) 12.

[34] A. Kumar, T. Hemg, K. Zeng, J. Ding, *Bipolar charge storage characteristics in copper and cobalt co-doped zinc oxide (ZnO) thin film*, ACS Applied Materials & Interfaces. 4 (2012) 527680.

[35] Y. Alivov, M. Chukichev, V. Nikitenko, *Green luminescence band of zinc oxide films copper-doped by thermal diffusion*, Semiconductors. 38 (2004) 31–35.

[36] D. Constantin, M. Apreutesei, R. Arvinte, A. Marin, O. Andrei, D. Munteanu, *Magnetron sputtering technique used for coatings deposition; technologies and applications*, 7th International Conference on Materials Science and Engineering – BRAMAT, 12 (2011) 1(31).

[37] V. Jain, X. Zhang, K. Hartwig, H. Wang, *Microstructure and Properties of Copper Thin Films on Silicon Substrates*, MS Thesis (Texas Agricultural and Mechanical University). (2007) 20-35.

[38] D. Depla, S. Mahieu, J. Greene, *Sputter deposition processes*, Materials Science. 1-13.

[39] D. Maurya, A. Sardarinejad, K. Alameh, *Recent developments in R.F. magnetron sputtered thin films for PH sensing applications*, Coatings. 4 (2014) 756-771.

[40] J. Böhlmark, *Fundamentals of high power impulse magnetron sputtering*, Linköping Studies in Science and Technology. (2005) 5-29.

[41] S. Swann, *Magnetron sputtering*, Physics and Technology.19 (1988).

[42] S. Ezugwu, G. Fanchini, P. Simpson, M. Cottam, M. Workentin, *Synthesis and characterization of copper nanoparticles and copper-polymer nanocomposites for plasmonic photovoltaic applications*, Electronic Thesis and Dissertation Repository. (2012) 1025.

[43] E. Särhammar, *Sputtering and characterization of complex multi-element coatings*, Digital Comprehensive Summaries of Uppsala Dissertations from the Faculty of Science and Technology. (2014) 1162.

[44] M. Duranleau, M. Kuntz, *Confocal cathode sputtering*, Semicore Equipment, Inc. (2013).

[45] L. Cui, H. Zhang, G. Wang, F. Yang, X. Kuang, R. Sun, J. Han, *Effect of annealing temperature and annealing atmosphere on the structure and optical properties of ZnO thin films on sapphire (0 0 0 1) substrates by magnetron sputtering*, Applied Surface Science. 258 (2012) 2479– 2485.

[46] F. Haque, K. Rahman, M. Islam, M. Rashid, M. Akhtaruzzaman, M. Alam, Z. Alothman, K. Sopian, N. Amin, *Growth optimization of Zns thin films by RF magnetron sputtering as prospective buffer layer in thin film solar cells*, Chalcogenide Letters. 11 (2014) 189-197.

[47] F. George, *Chromium-free conversion coating of aluminum-copper alloys*, School of Materials. (2010) 114-121.

[48] D. VIJ, *Handbook of applied solid state spectroscopy*, Springer Science+Business Media. (2006) 2006923765.

[49] S. Hofmann, *Auger- and x-ray photoelectron spectroscopy in materials science*, Springer Series in Surface Sciences 49. (2013) 0931-5195.

[50] L. Scudiero, *X-ray photoelectron ray photoelectron spectroscopy (XPS)*, Washington State University. 5 2669.

[51] A. Khalid, A. Khan, M. Anwar, *X-ray fluorescence (XRF) spectrometry for materials analysis and discovering the atomic number*, LUMS School of Science and Engineering. (2011) 4-5.

[52] N. Sung, S. Kang, H. Shin, H. Lee, I. Lee, *Cu doping effect on the electronic and optical properties of Cu-doped ZnO thin films fabricated by radio frequency magnetron sputtering*, Thin Solid Films. 547 (2013) 285-288.

[53] M. Oztas, M. Badir, *Thickness dependence of structural, elctrical and optical properties of sprayed ZnO:Cu films*, Thin Solid Films. 516 (2008) 1703–1709.

[54] D. Wang, J. Zhou, G. Liu, *The microstructure and photoluminescence of Cu-doped ZnO nano-crystal thin films prepared by sol-gel method*, Journal of Alloys and Compounds. 487 (2009) 545–549.

[55] A. Naumkin, A. Vass, S. Gaarenstroom, C. powell, *NIST x-ray photoelectron spectroscopy database, NIST standard reference database 20*, National Institute of Standards and Measures. (2012).

[56] A. Hartmann, M. Puchert, R. Lamb, *Influence of copper dopants on the resistivity of ZnO films*, Surface and Interface Analysis. 24 (1996) 671-674.

[57] A. Sobas, A. Galeckas, M. Sunding, S. Diplas, A. Kuznetsov, *An investigation of Fe-doped ZnO thin films grown by magnetron sputtering*, Physica Scripta T. 141 (2010) 014004.

[58] S. Pearton, D. Norton, K. Ip, Y. Heo, T. Steiner, *Recent progress in processing and properties of ZnO*, Progress in Materials Science. 50 (2005) 293–340.

[59] C. Soci, A. Zhang, B. Xiang, S. Dayeh, D. Aplin, J. Park, X. Bao, Y. Lo, D. Wang , *ZnO nanowire UV photodetector with high internal gain*, Nano Letters. 7 (2007) 1003-1009.

[60] G. Poongodi, P. Andan, R. Kumar, R. Jayavel, *Studies on visible light photocatalytic and antibacterial activites of nanostructured cobalt ZnO thin films prepared by sol-gel coating method*, Spectrochimica Acta Part A: Molecular and Biomolecular Spectroscopy. 148 (2015) 237–243.

[61] Y. Nakano, T. Morikawa, T. Ohwaki, Y. Taga, *Deep-level characterization of N-doped ZnO films prepared by reactive magnetron sputtering*, Applied Physics Letters. 87 (2005) 232104.

[62] P. Misra, P. Sahoo, P. Tripathi, V. Kulkarni, R. Nandedkar, L. Kukreja, *Sequential pulsed laser deposition of $Cd_xZn_{1-x}O$ alloy thin films for engineering ZnO band gap*, Applied Physics A. 78 (2004) 37-40.

[63] P. Liu, P. Shao, *Electron structure and band gap engineering of ZnO based semiconductor alloy films*, Molecular Simulation. 39 (2013) 1007-1012.

[64] S. Ray, *Preparation of copper oxide thin films by the sol-gel-like dip technique and study of their structural and optical properties*, Solar Energy Materials & Solar Cells. 68 (2001) 307-312.

[65] C. Moon, S. Wei, Y. Zhu, G. Chen, *Band-gap bowing coefficient in large size mismached II-VI alloys: first-priciples calculations*, Physical Review B. 74 (2006) 233202.

[66] H. Sutanto, S. Wibowo, I. Nurhasanah, E. Hidayanto, H. Hadiyanto, *Ag doped ZnO thin films synthesized by spray coating technique for methylene blue*

photodegradation under UV irradiation, International Journal of Chemical Engineering. (2016) 6195326.

[67] B. Singh, S. Tripathi, *Influence of Bi concentration on structural and optical properties of Bi doped p-type ZnO thin films prepared by sol–gel method*, Journal of Materials Science: Materials in Electronics. 27 (2016) 2360-2366.

[68] G. Li, X. Zhu, X. Tang, W. Song, Z. Yang, J. Dai, Y. Sun, X. Pan, S. Dai, *Doping and annealing effects on ZnO:Cd thin films by sol-gel method*, Journal of Alloys and Compounds 509 (2011) 4816–4823.

[69] A. Acharya, S. Moghe, R. Panda, S. Shrivastava, M. Gangrade, T. Shripathi, D. Phase, V. Ganesan, *Effect of Cd dopant on electrical and optical properties of ZnO thin films prepared by spray pyrolysis route*, Thin Solid Films. 525 (2012) 49–55.

[70] F. Xian, L. Xu, X. Wang, X. Li, *Crystallographic, optical and magnetic properties of Co-doped ZnO thin films synthesized by sol-gel route*, Crystal Research and Technology. 47 (2012) 423 – 428.

[71] N. Tarwal, K. Guravd, T. Kumar, Y. Jeong, H. Shim, I. Kim, J. Kim, J. Jang, P. Patil, *Structure, x-ray photoelectron spectroscopy and photoluminescence investigations of the spray deposited cobalt doped ZnO thin films*, Journal of Analytical and Applied Pyrolysis. 106 (2014) 26–32.

[72] A. Kulandaisamy, C. Karthek, P. Shankar, G. Mani, J. Rayappan, *Tuning selectivity through cobalt doping in spray pyrolysis deposited ZnO thin films*, Ceramics International. 42 (2016) 1408-1415.

[73] P. Kumar, C. Kartha, K. Vijayakumar, F. Singhb, D. Avasthi, *Effect of fluorine doping on structural, electrical and optical properties of ZnO thin films*, Materials Science and Engineering B. 117 (2005) 307–312.

[74] Z. Chen, L. Zhuge, X. Wu, Y. Meng, *Initial study on the structure and optical properties of* $Zn_{1-x}Fe_xO$ *films*, Thin Solid Films. 515 (2007) 5462–5465.

[75] A. Rambu, V. Nica, M. Dobromir, *Influence of Fe-doping on the optical and electrical properties of ZnO films*, Superlattices and Microstructures. 59 (2013) 87–96.

[76] M. Ahmad, E. Ahmed, Z. Hong, Z. Iqbal, N. Khalid, T. Abbas, I. Ahmad, A. Elhissi, W. Ahmed, *Structural, optical and photocatalytic properties of hafnium doped zinc oxide nanophotocatalyst*, Ceramics International. 39 (2013) 8693–8700.

[77] M. Caglar , S. Ilican, Y. Caglar, *Influence of dopant concentration on the optical properties of ZnO: In films by sol–gel method*, Thin Solid Films. 517 (2009) 5023–5028.

[78] C. Manoharan, G. Pavithra, S. Dhanapandian, P. Dhamodharan, *Effect of In doping on the properties and antibacterial activity of ZnO films prepared by spray pyrolysis*, Spectrochimica Acta Part A: Molecular and Biomolecular Spectroscopy. 149 (2015) 793–799.

[79] J. Jin, G. Chang, Y. Zhou, X. Zhang, D. Boukhvalov, E. Kurmaev, A. Moewes, *X-ray absorption and emission spectroscopic investigation of Mn doped ZnO films*, Applied Surface Science. 257 (2011) 10748– 10751.

[80] M. Naouar, I. Ka, M. Gaidi, H. Alawadhi, B. Bessais, M. El Khakani, *Growth, structural and optoelectronic properties tuning of nitrogen-doped ZnO thin films synthesized by means of reactive pulsed laser deposition*, Materials Research Bulletin. 57 (2014) 47–51.

[81] J. Lv, K. Huang, X. Chen, J. Zhu, C. Cao, X. Song, Z. Sun , *Optical constants of Na-doped ZnO thin films by sol–gel method*, Optics Communications. 284 (2011) 2905–2908.

[82] R. Siddheswaran, M. Netrvalová, J. Savková, P. Novák, J. Oc˘enášek, P. Šutta, J. Jr, R. Jayavel, *Reactive magnetron sputtering of Ni doped ZnO thin film: Investigation of optical, structural, mechanical and magnetic properties*, Journal of Alloys and Compounds. 636 (2015) 85–92.

[83] C. Prajapati, A. Kushwaha, P. Sahay, *Optoelectronics and formaldehyde sensing properties of tin-doped ZnO thin films*, Applied Physics A. 113 (2013) 651–662.

Vitae

Name: SAEED ABDULLAH SAEED BAQRAF

Nationality: YEMENI

Date of Birth: 10/15/1987

Email: saeed201071@gmail.com

Address: Mukalla – Hadhramout - Yemen

Education:

- M.Sc. in Physic science, King Fahd University of Petroleum and Mineral (KFUPM-KSA).
- B.Sc in Physics science from Faculty of science, Hadramout University of Science and Technology.

Experience:

- A Physics science and math science teacher in ministry of education.
- A Physics science and math science teacher in prive schools.
- A Physics science and math science teacher in various institutes in Mukalla.

Publications:

- M. F. Al-Kuhaili, S. A. Baqraf, S. M. A. Durrani, A Substantial linear red shift in the band gap in heavily copper doped zinc oxide thin films produced by co-sputtering, Journal of Materials Science: Materials in Electronics. (2017) DOI 10.1007/s10854-017-7126-9.